STRUCTURE-FUNCTION OF THE CYTOCHROME B_6F COMPLEX IN OXYGENIC PHOTOSYNTHESIS: MOLECULAR CONTROL OF ELECTRON TRANSPORT AND THERMODYNAMIC ANALYSIS OF THE INTERACTION OF A PROPOSED PROTEIN LIGAND

by

Jillian Ness

A Thesis

Submitted to the Faculty of Purdue University

In Partial Fulfillment of the Requirements for the degree of

Master of Science

Department of Biological Sciences

West Lafayette, Indiana

August 2020

THE PURDUE UNIVERSITY GRADUATE SCHOOL

STATEMENT OF COMMITTEE APPROVAL

Dr. William A. Cramer, Chair

Department of Biological Sciences

Dr. Nicholas Noinaj

Department of Biological Sciences

Dr. Carol B. Post

Department of Medicinal Chemistry and Molecular Pharmacology

Department of Biological Sciences

Approved by:

Dr. Janice Evans

ACKNOWLEDGMENTS

Thank you to Ravi, Karthik, and Run Run for your all of your helpful discussions.
Thank you Eric, Claire, and my family for your love and support!

TABLE OF CONTENTS

LIST OF TABLES

LIST OF FIGURES

LIST OF SYMBOLS, ABBREVIATIONS AND NOMENCLATURE

aadA, aminoglycoside-3'-adenyl transferase gene cassette for spectinomycin resistance

ATP, adenosine triphosphate

BME, β-mercaptoethanol

C. reinhardtii, Chlamydomonas reinhardtii

CET, cyclic electron transport

Chl-a, chlorophyll-a

Cyt, cytochrome

DDM, n-dodecyl *β*-d-maltoside

DTT, dithiothreitol

DBIMB, 2,5-dibromo-3-methyl-6-isopropylbenzoquinone

FCCP, carbonyl cyanide *p*-trifluoromethoxy-phenylhydrazone

Fd, ferredoxin

FNR, ferredoxin:NADP oxidoreductase

HEPES, 2-[4-(2-hydroxyethyl)piperazin-1-yl]ethanesulfonic acid

ISP, Rieske Iron-Sulfur Protein

K_d, dissociation constant

LET, linear electron transport

LHC, light harvesting complex

M. laminosus, Mastigocladus laminosus

n-side/p-side, electrochemically negative and positive side of the membrane with respect to direction of proton translocation

NADP+, nicotinamide adenine dinucleotide phosphate

Ni-NTA, nickel nitrilotriacetic acid

OD, optical density

petD, subunit IV gene

PC, plastocyanin

PCR, polymerase chain reaction

PDB, protein data base

Phe, Phenalanine.

PGR5, Proton Gradient Regulator 5

PGRL1, Proton Gradient Regulator-Like 1

PSI, PSII, photosystem I and II reaction center complex

PQ, plastoquinone

PQH_2, plastoquinol

Q_p, quinol binding (oxidation) site in cytochrome b_6f on electrochemically positive side of membrane, also referred to as Q_o

s/sec, second

$Spec^R$, spectinomycin resistance

subIV, subunit IV

SDS-PAGE, sodium dodecyl sulfate-polyacrylamide gel electrophoresis

TDS, tridecyl-stigmatellin

TMH, trans-membrane helix

Trp, tryptophane

Tyr, tyrosine

UDM, n-undecyl-beta-maltoside

WT, wild type

[2Fe-2S], iron-sulfur cluster

ΔA, absorbance change

ΔG, change in Gibbs free energy

ΔH, change in enthalpy

ΔS, change in entropy

ABSTRACT

In the first study presented here, the 2.5 Å crystal structure[1] of the cytochrome b_6f complex obtained from the cyanobacterium *Nostoc sp. PCC 7120* (pdb 4OGQ) was used as a guide for modification by site-directed mutagenesis in the cyanobacterium *Synechococcus* sp. PCC 7002 of the rate-limiting step in the central electron transport/proton translocation chain of oxygenic photosynthesis. This step is associated with the oxidation and deprotonation of plastoquinol on the electrochemically positive (p) side of the membrane. The mutagenesis strategy is based on structure studies of the b_6f complex in the absence and presence of quinol analogue inhibitors which bind and inhibit electron transport on the p-side of the thylakoid membrane. The strategy focused on two conserved prolines located on the p-side of the F-helix, proximal to the C-helix, in subunit IV of the seven subunit cytochrome b_6f complex. These prolines, residues 105 and 112 in the F-helix, are seen in the crystal structure to cause a bend in this helix away from the C-helix in the cytochrome *b* subunit. Thus, they are predicted to increase the portal aperture for the plastoquinol generated in the photosystem II reaction center complex that serves as the electron-proton donor to the [2Fe-2S] iron-sulfur protein and the p-side *b*-heme. Changing the two prolines to alanine resulted in a decrease of 30-50 % in the log-phase growth rate of the cell culture and reduction of photo-oxidized cytochrome *f*.

The second study examines the binding thermodynamics of the cytochrome b_6f complex and a purposed binding partner, PGRL1, using isothermal titration calorimetry. Proton Gradient Regulation-Like 1 (PGRL1) is thought to be necessary for efficient cyclic electron transfer, however, it's mechanistic role is unknown. Here we examined for PGRL1 and cytochrome b_6f complex binding and found there was no detectable interaction, indicating that PGRL1 is not a direct quinone/cyt b_6f electron cofactor.

CHAPTER 1. STRUCTURE-BASED CHANGE OF THE RATE-LIMITING STEP IN THE ELECTRON TRANSPORT CHAIN OF OXYGENIC PHOTOSYNTHESIS

1.1 Introduction

The structural basis of the rate limitation of oxygenic photosynthesis is central to understanding the function of the individual macromolecules in the photosynthetic apparatus, and possible application of this knowledge to agricultural productivity[1, 2]. Knowledge of the atomic structure of the hetero-oligomeric cytochrome b_6f complex in the photosynthetic electron transport chain[3-5] is applied here to a strategy for limitation of the rate of oxygenic photosynthesis involving electron and proton transfer to the b_6f complex, proposed earlier on the basis of less precise information on the structure of the complex.[6] An experimental proof of this hypothesis is provided in the present study.

Among the environmental parameters that determine the efficiency of photosynthesis, the incident light intensity and its spectral distribution are major determinants. Light harvesting in plants and oxygenic photosynthetic microorganisms utilize a 400-700 nm spectral band of visible light, dictated by the absorbance spectra of the bulk antenna chlorophyll and auxiliary light harvesting pigments. In addition to incident light intensity and its spectral distribution,[7,8] limitations to the level of photosynthetic activity are imposed by the rate of carbon dioxide (CO_2) fixation which requires the energy source, ATP, and the effective reductant, NADPH, generated in the light.[9] When the CO_2 level is sufficient, a limitation on the rate of photosynthesis is imposed by the rate of synthesis of ATP and NADPH. These rate-limiting compounds are generated via the free energy resulting from exergonic electron transport and the proton gradient generated by the oxidation of water and the plastoquinol hydrogen carrier. A consequence of the dependence of the efficiency of the rate of CO_2 fixation and net photosynthesis on ribulose-1,5-bisphosphate carboxylase[1,9] is an inter-dependence of rates of photosynthesis and photorespiration.[10]

Under conditions of high incident light intensity and favorable ambient conditions for CO_2 fixation, trans-membrane proton translocation associated with the oxidation of plastoquinol can be rate-limiting. The plastoquinol-mediated reduction of cytochrome *f* and the high potential Rieske iron-sulfur (2Fe-2S) protein, located in the electron transport chain connecting the two reaction center complexes, is the electron transfer step associated with the rate-limitation in the electron

transport chain that links the two photosystems.[11-17] This charge transfer step can be measured most readily by quinol-mediated changes in the rate of cytochrome *f* reduction, which is the terminal acceptor in the b_6f complex of electrons donated to the complex by plastoquinol. Redox changes associated with cytochrome *f* turnover resulting from reduction by plastoquinol, measured in intact cells of cyanobacteria[18] and green algae[19, 20] by light flash-dependent kinetic difference spectroscopy, occur with a characteristic reaction time of a few milliseconds.

The present study is focused on the protein structure basis of the rate limitation of photosynthetic electron transport in the cyanobacterium, *Synecococcus* sp. PCC 7002, considered to have representative parameters of plant photosynthetic electron transport, and site-based mutagenesis to direct genetically specified structure changes proposed to alter the rate-limiting step of the non-cyclic electron transport chain. Specifically, the entry-exit portal of plastoquinol/quinone in the lumen (p)-side core of the cytochrome b_6f complex was changed in the cyanobacterium *Synecococcus* by site-directed mutagenesis to create a modified intra-membrane pathway for plastoquinol-mediated electron/proton transfer.

The structural basis for prediction of sites in the b_6f complex responsible for the rate-limiting step associated with oxidation of plastoquinol and the associated trans-membrane proton transfer in the electron transport chain was initially based on crystallographic structures of the individual major subunits, cytochrome *f* [21] and the Rieske iron-sulfur protein.[22] Subsequently, crystal structures were obtained of the intact b_6f complex from the moderately thermophilic cyanobacterium, *M. laminosus* (PDB 1VF5, 2E74),[23] and the green alga, *C. reinhardtii* (PDB 1Q90).[24] Additional crystal structure information, essential for the background of the present study, was obtained of the *M. laminosus* b_6f complex in the presence of the inhibitors stigmatellin (PDB 4PV1), tridecyl-stigmatellin (PDB 2E76, 4PV1, 4H13), and NQNO (PDB 2E75).[25] These structure studies culminated in the highest resolution (2.5 Å) crystal structure (pdb 4OGQ) obtained thus far of the hetero-oligomeric b_6f complex (molecular weight 225 kDa exclusive of prosthetic groups and bound lipid), and twenty-three lipid binding sites per monomer, for the b_6f complex obtained from the cyanobacterium *Nostoc* sp. PCC 7120[26] (Figure 1.1).

The dimeric hetero-oligomeric structure described in Figure 1.1 contains eight polypeptide subunits: (**i**) those containing redox cofactors are electron transport proteins petA (cyt *f* subunit, one trans-membrane helix, (**ii**) petB (cytochrome b_6, 4 TMH), (**iii**) petC (Rieske 2Fe-2S protein, with a unique 'domain-swapped' TMH, and (**iv**) petD or subunit IV (suIV, 3 TMH) which

corresponds to the C-terminal half of the cytochrome *b* subunit of the cytochrome bc_1 complex[27]. The protein core of the cytochrome complex in each monomer of the dimeric complex contains five permanently bound metallo-protein redox prosthetic groups (four hemes, *f*, b_p, b_n. and c_n, and one 2Fe-2S cluster). The dimeric complex also contains four small (3-4 kDa) hydrophobic peptides, petG, L, M, and N, a hydrophobic 'picket fence,' which flank each monomer, and is a unique sub-structure in the entire family of integral membrane proteins (Figure 1.1). The trans-membrane helices in Figure 1.1 are shown as ribbons, and the Rieske [2Fe-2S] cluster as an orange-yellow sphere-stick. A single copy of a unique chlorophyll a (Chl *a*) and ß-carotene, each with an as yet undefined function in the b_6f complex, shown in green and yellow, respectively, is present in each monomer.

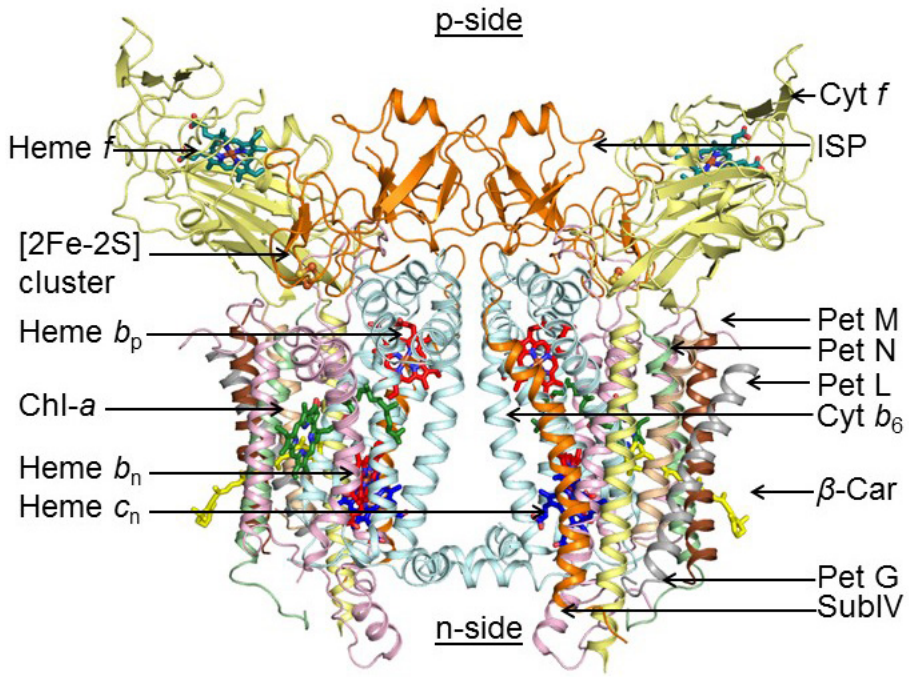

Figure 1.1. *Ribbon diagram of cytochrome b_6f lipoprotein complex obtained from the cyanobacterium* Nostoc *sp. PCC 7120.*[4] The 2.5 Å structure, a symmetric dimer with C2 symmetry including 23 lipid binding sites per monomer, has been described (pdb 4OGQ). The homo-dimeric complex contains, per monomer, 13 trans-membrane α-helices and 7 prosthetic groups (5 hemes, 1 chlorophyll *a,* and 1 β-carotene). In addition, each monomer contains four small (3.4–4.1 kDa) Pet M, N, L, and G subunits), and 7 prosthetic groups [5 redox (4 hemes: *f*, b_n, b_p, c_n), 1 FeS cluster], one Chl *a* with its phytyl chain wrapped around the F-helix of subunit IV in the b_6f complex, and one β -carotene which is seen (in yellow) to protrude 11 Å from the complex. With redox co-factors, the molecular weight of the complex from *spinacea*, including redox co-factors, is 268 kDa determined by mass spectrometry (pers. communication, C. Bechera). Figure reproduced from original.[5]

From examination of the oxidation site of plastoquinol (Figure 2.1A) within each monomer of the complex, it can be seen that the rate limitation of plastoquinol oxidation could be a consequence of the steric constraint resulting from the requirement imposed by the protein

structure that the plastoquinol and plastoquinone pass through a narrow portal ("Q_p portal"), approximately 11 Å in length, on the electrochemically positive (p) side of the complex (pdb 4OGQ) (Figure 1.2A). The sites in the structure of the b_6f complex which interact with the integral domain of the iron-sulfur protein (ISP), with the other subunits of the complex, and the entry/exit portal of the quinone/quinol (Figure 1.2B) into the electrochemically positive side of the b_6f complex, have been identified from the solved structure of the cytochrome complex with quinol analogue inhibitors.[25]

The 'Q_p portal' provides the entry/exit channel for transit of the reduced quinol/quinone to a position sufficiently proximal to allow electron transfer to the [2Fe-2S] cluster of the iron-sulfur protein (ISP), and proton transfer to the external electrochemically positive side of the membrane. Details of the charge transfer mechanism from the quinol to the iron-sulfur protein have been considered most carefully in a discussion of the mechanism for the purple photosynthetic bacterium, *Rps. sphaeroides*.[28] The exit of the oxidized plastoquinone from the portal, 11 Å in length, and subsequently from the b_6f complex has been described in an analysis of the p-side intra-protein pathway of quinol-quinone traffic, which implies passage from the inter-protein domain of the membrane into the inter-monomer lipid/water-filled space of the dimeric complex.[5,29] An unanticipated aspect of the model and simulated exit pathway of the plastoquinone from its p-side charge transfer site is that it was found to be hindered by the presence of the phytyl chain of the unique chlorophyll *a* molecule, wrapped around the 'F'-trans-membrane helix in subunit IV of the b_6f complex (Figure 1.2B) .[29]

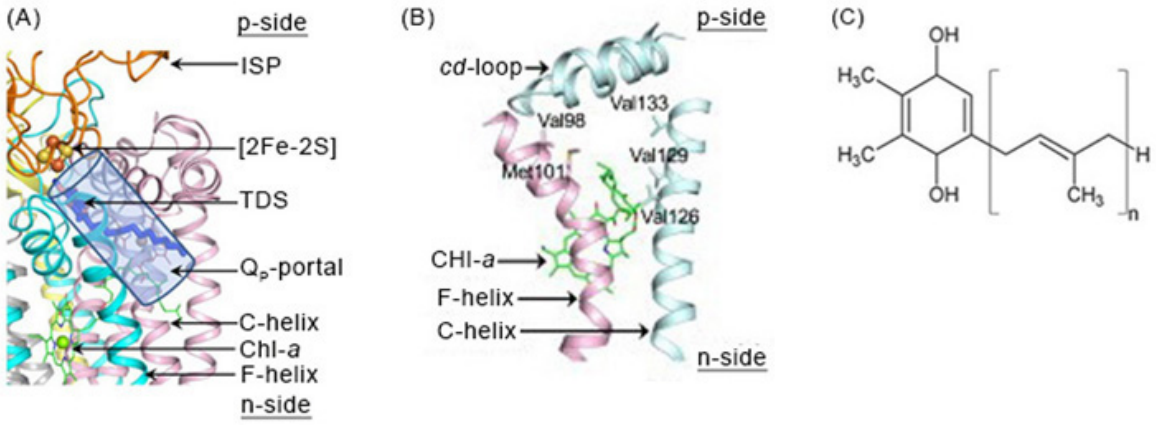

Figure 1.2. *The inferred p-side quinone entry/exit portal* **(A)** Electrochemically positive (lumen, p-side) plastoquinone (Qp)-portal in the cytochrome b_6f complex, shown to be occupied by the quinone analog, tridecyl-stigmatellin, TDS (PDB 4H13); quinone analog, tridecyl-stigmatellin (TDS), in a stick representation, shown to bind in the portal highlighted as a blue cylinder. **(B)** p-side trans-membrane structure elements of the cytochrome b_6f complex inferred to be in the pathway of plastoquinol/plastoquinone entry-exit.[6] **(C)** Model of plastoquinone with n = 9 isoprenoid groups at position 3 on the benzenoid ring.

On the basis of models and hypotheses[5] derived from the crystal structure of the b_6f complex, the structure information described above has been employed in the present study as the basis for a strategy that utilizes site-directed mutagenesis to modify the plastoquinol-mediated rate-limiting electron transfer step in the intra-membrane electron transport chain of the cyanobacterium, *Synecococcus* sp. PCC 7002.

The intra-monomer quinone entry portal is bounded by the 'C' and 'F' trans-membrane α-helices, associated, respectively, with the cytochrome *b* and subunit IV components of the complete b_6f complex (Figure 1.1, 1.2A). It was previously suggested[6] that proline residues of interest in the mechanism of plastoquinone translocation within the b_6f complex are conserved in the 'F' helix of subunit IV at positions 105 and 112 in cyanobacteria, the green alga *C. reinhardtii*, and plants (Figure 2.1B). The unique dihedral angle of proline amino acids results in a strain in the alpha-helices in which they reside which distort their conformation to create the aperature of the port;.[30] Proline residues 105 and 112, which are known from the 2.5 Å crystal structure (pdb 4OGQ) to reside on the same side of the subunit IV 'F' trans-membrane helix, result in a bend of the 'F'-helix away from the 'C'-helix (Figure 1.2B, 1.3A, 1.3C). The space between the trans-membrane 'F' and 'C' helices on the p- (lumen) side of the membrane defines an apparent passage of plastoquinol/quione to/from the p-side quinone portal shown in Figure 1.2A. It is predicted that if the proline mutations structurally contribute to the opening of the portal and they are mutated to non-helix breaking amino acids, i.e. alanines, then the rate of quinol oxidation will significantly decrease due to diminished space within the quinol portal. The validity of of this inference is tested in the present study.

1.2 Results and Discussion

1.2.1 Results

It is proposed that under conditions when the light intensity is not limiting, the rate limitation in the linear electron transport chain can be defined and limited by steric constraints in the structure of the entry/exit portal of quinol/quinone to/from the iron-sulfur (2Fe-2S) protein and electron/proton transfer from plastoquinol to the cluster.

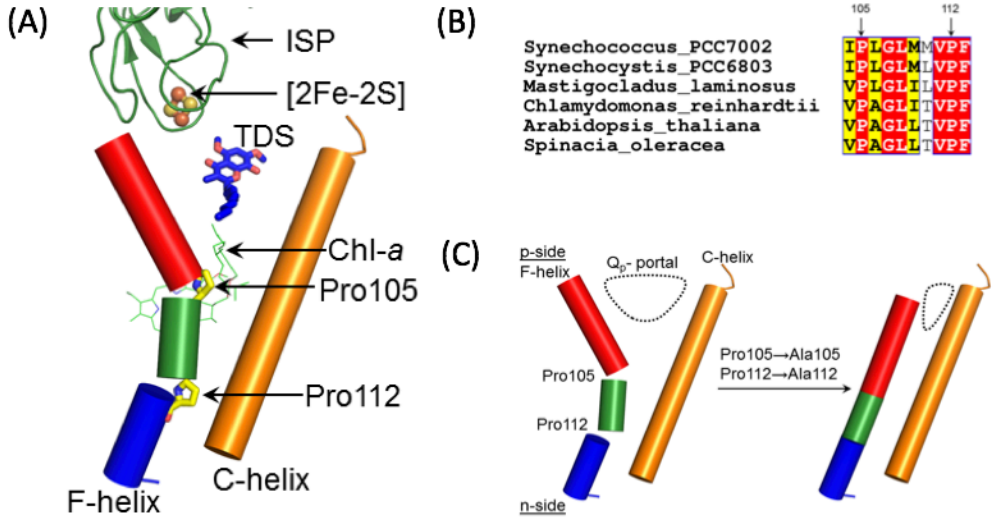

Figure 1.3. *Conservation of proline residues 105 and 112 in the F-helix of the Q_p portal of the cytochrome b_6f complex.* **(A)** Structure basis of entry/exit pathway to p-side portal (Q_p) for plastoquinol/one. Pro105 and Pro112 determine a structure of the F-helix that generates space for the Qp-portal. C and F-helices are shown as cylinders. **(B)** Multiple sequence alignment[16] showing conservation of Pro105 and Pro112 residues in F-helix of subunit IV. Color code: red, yellow, white, complete, partial, and no conservation. Sequence alignment done across three cyanobacteria, a green alga (*C. reinhardtii*), spinach *oleraceae*, and *Arabidopsis*) performed in Clustal-Omega.[31] UNIPROT accession numbers of subunit IV sequences: *Synechococcus* PCC 7002, P28057; *Synechocystis* PCC 6803, P27589; *M. laminosus*, P83792; *C. reinhardtii*, P23230; *A. thaliana*, P56774; *S. oleracea*, P00166. Amino acid sequence of p-side segment, the subunit IV F-helix showing conservation of proline residues at positions 105, 112 (black arrows). **(C)** Schematic representation of Pro to Ala mutation in the Q_p-portal. C and F helices of b_6f complex shown as cylinders. Conformation change of F-helix relative to the C-helix shows a decrease in the Qp portal aperture that is predicted to result from changing Pro 105 and Pro 112 to Ala. p, n, electrochemically positive and negative sides of a membrane. Color code: C-helix, orange; F-helix, blue-green-red (left).

Pro105 and Pro 112 were changed to the relatively small residue Ala, which is predicted to cause removal of the bend of the F-helix (Figure 1.2C), a decrease in size of the Q-portal and, thereby, decreased access of plastoquinol to the high potential electron acceptors, the Rieske high potential iron-sulfur protein (via 2Fe-2S cluster in the ISP protein, Figure 1.2) and cytochrome *f* to which it is closely coupled, on the electrochemically positive ('p'), side of the membrane. From general knowledge of the structural basis of the rate-limiting step in the 'non-cyclic' electr

on transport chain, discussed above, it is hypothesized that the consequence of the mutational changes associated with the P105A-P112A double mutant of *Synecococcus* would be a decrease in: the growth rate of the culture (Figure 1.4) and the rate of reduction in the dark of cytochrome *f* after photo-oxidation by a short (ca. 10 μs) Xenon light flash incident upon a suspension of intact *Synecococcus* cells (Figure 1.5).

Growth Rate; Data collection aided by K. Effinger. The growth rate in illuminated cultures of the P105A-P112A mutant relative to the wild type is smaller by more than two-fold in the early-mid phase of the exponential growth (Figure 1.4)

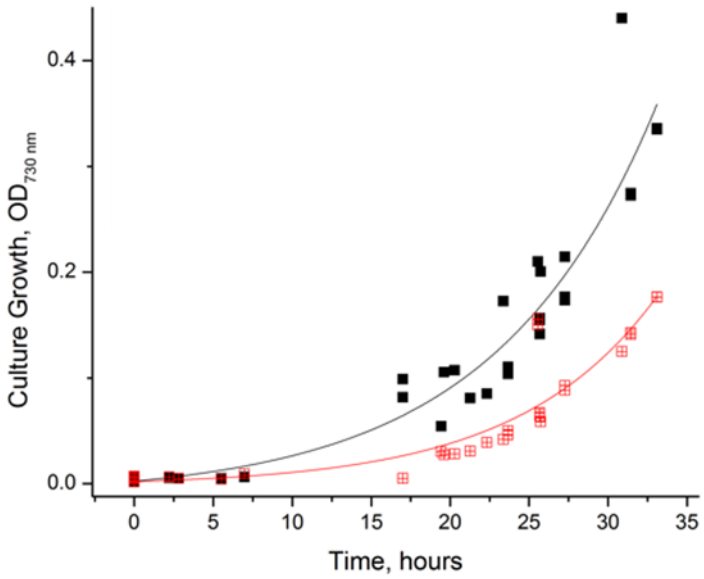

Figure 1.4. *Growth rate of wild type (black) and P105A-P112A mutant (red) of Synechococcus sp. PCC 7002 determined (n = 4).* Growth of cultures in medium A (Methods, Ch. 1.4.1) was measured by absorbance at 730 nm. Data fit to exponential functions: slopes of growth functions for wild type and P105A-P112A mutant are 1.4 x 10^{-3} $e^{t/10.2}$ and 4.5 x 10^{-4} $e^{t/.8.8}$. Samples from culture flask diluted 10-fold prior to measurement of absorbance. Growth rate of wild type relative to mutant is 2.2 :1 when elapsed growth time is 24 hours.

Rate of cytochrome *f* reduction. The cytochrome oxidation state was monitored through its absorbance change in the heme α-band region of the spectrum at 556 nm relative to the absorbance change at the reference wavelength of 540 nm. The half-times of the quinol-mediated increase in absorbance for the wild type and mutant associated with the reduction of cytochrome *f*, proceeding after flash-induced oxidation of the photosystem I reaction center are, respectively, 6.7 ± 1.3 msec and 20.7 ± 5.2 msec (Figure 1.5A). In addition, this cyt *f* redox kinetic study serves to provide a control to ensure equal concentrations of b_6f in the double mutant cell population relative to the wild type; the dimeric b_6f population concentrations were off by .4 μM, indicating the mutant cyt b_6f is folded and transported to the thylakoid membrane similar to the wild type (mM extinction coefficient for difference peak, 25 mM cm^{-1}). the change in absorbance of each cyt f redox Association of the spectral response in Figure 1.5A with cytochrome *f*, whose characteristic α-

band absorbance peak at 556 nm, measured with intact cells of *Synechococcus*,[18] is displayed in a reduced minus oxidized difference spectrum whose peak is at 556 nm (Figure 1.5B). Any distortions in the well-characterized cyt *f*/c_6 difference spectrum of P105A-P112A double mutant would indicate a redox insensitive (non-functional) cyt *f*/c_6.; however, the classical spectrum is observed of the mutant, indicating a functional quinol oxidation pathway.

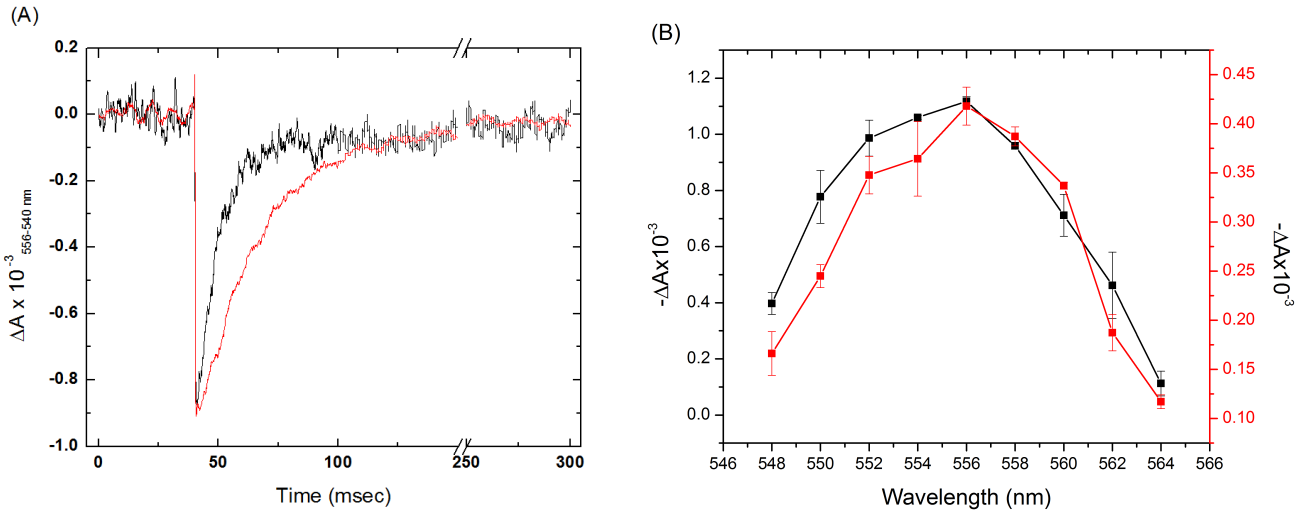

Figure 1.5. *Kinetics of* Synechococcus sp. *PCC 7002 cytochrome f/c_6 redox changes in vivo.* **(A)** Kinetics of flash-induced oxidation and subsequent dark reduction of cytochrome *f*/c_6 redox changes *in vivo* average traces of wild type (black trace) and P105A-P112A mutant (red trace) of the cyanobacterium *Synechococcus sp.* PCC 7002 (40 µM chlorophyll-a content). Each trace is an average of 100 flash-induced absorbance changes, 2 s between flashes. Suppression of 60 Hz background noise employed software described elsewhere.[32] Cytochrome oxidation state monitored through the absorbance change at 556 nm relative to that at the 540 nm reference wavelength. Cells suspended as described in Methods. Xenon light flash (half-width, 5-10 µsec) was imposed on sample 40 msec after the flash trigger pulse. Average half-time and standard deviation of cytochrome *f* reduction (n = 7 trials) after flash-induced oxidation: wild type, 6.7 ± 1.3 msec; P112A /P105A mutant, 20.7 ± 5.2 msec. **(B)** Action spectra and SEM (standard error mean) over the wavelength interval 548-564 nm, referenced to the 540 nm isosbestic wavelength, of flash-induced absorbance changes in the cytochrome α-band region of wild type (n=2), 40 µM (in black), P105A-P112A mutant (n=2), 20 µM chlorophyll (in red) *Synechococcus sp.* PCC 7002. Difference spectra of flash-induced oxidation show the spectral change to have an absorbance maximum at 556 nm, characteristic of cyt *f*/c_6 in *Synecococcus*.[18]

Discussion The above studies define a test of the ability to experimentally alter the rate of oxygenic photosynthesis through site-directed changes of specific amino acid residues in the cytochrome b_6f complex, specifically in a niche in the p-side quinone entry pathway. From the 2.5 Å crystal structure of the cyanobacterial b_6f complex[4] and its structure with a bound p-side quinone analogue inhibitor,[25] the sub-structure or space between the 'C' and 'F' trans-membrane helices in the cytochrome complex (Figure 1.2B, 1.3C) was inferred to be in the passage for transfer of plastoquinol from the photosystem II reaction center to the p-side portal and oxidation site in the

b_6f complex associated with the rate-limiting step of electron transport. Therefore, It is considered to be a site for control and regulation. Corroboration of this inference is based on the effect of site-directed change of two proline residues at this site on the rate of (**i**) growth of the cell culture, and (**ii**) the rate of photosynthetic oxygen evolution, and (**iii**) reduction of photo-oxidized cytochrome *f*. A search was also made for change in the rate of flash-induced reduction of a heme of the cytochrome b_6 component of the b_6f complex.[33] No significant amplitude corresponding to reduction of *b* heme with an absorbance peak at 563 nm could be seen, implying either that (**i**) the *b*-hemes in the cyanobacterial complex are predominantly in a reduced state in the growing cell culture, or (**ii**) that the flash-induced *b* heme is re-oxidized much more rapidly than it is reduced.

Immediate consequences of the demonstration in the present study of the ability to perform designed mutagenesis of the p-side quinone portal in the cytochrome b_6f complex are: **(i)** use of a similar logic and methodology to modulate the same p-side portal function to establish an increased rate of electron transport and photosynthetic productivity; **(ii)** carry out this gene transfer and mutagenesis in higher plants.[34] It can be proposed to accomplish this transformation through a design logic involving the F and C trans-membrane helices similar to that used in the present study, based on details (Figure 1.2B, 1.3C) of the crystal structure of the b_6f complex.[4]

1.3 Future Directions

Immediate implications of the present study to perform designed mutagenesis of the p-side quinone portal in the cytochrome b_6f complex is: (i) the possibility of using a similar logic and methodology to modulate the same p-side portal function so as to establish an increased rate of electron transport and photosynthetic productivity; (ii) carry out this gene transfer and mutagenesis in the chloroplasts of higher plants.[29] It can be proposed to accomplish this transformation through a design logic involving the F and C trans-membrane helices (Fig. 2C), as suggested previously.[26] The motivation in such a project would be to engineer and accelerate the rate of photosynthetic electron transport in plants in order to accomplish an increase in agriculturally relevant plant productivity. Although the structure of the photosynthetic apparatus in cyanobacteria, algae, and plants has evolved to its present functional state over the millenia, fine-tuning of the plant growth apparatus by genetic engineering (e.g., genetically modified crops, or GMO) is well-established.[34]

Mutations have been attempted over the last year to insert prolines at sites 108, 101, and a double mutant at 101/108 in *Synechococcus* sp. PCC 7002 (Figure 1.6); however, further study is

needed as the organisms grew for several days until the colonies bleached and died. Perhaps if the proline residues are too drastic a change so as to be deleterious, future studies can be directed towards modifying the bulky, conserved residues at sites Ile109 and Phe113 to smaller residues (i.e. Ala) (Figure 1.3B). This secondary mutagenesis method could reduce steric clashing of the portal with the bulky PQ molecule.

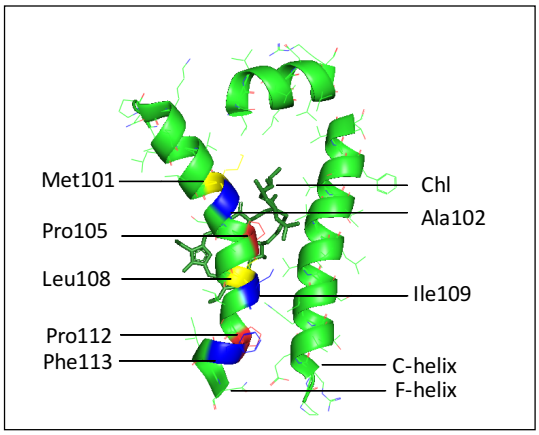

Figure 1.6. *Schematic of the Q_p portal of the cytochrome b_6f complex with highlighted residues of interest.* Residues that have been modified successfully and tested (red); residues that have been modified and did not survive (yellow); candidate residues for site-directed mutagenesis (blue). Ile109 and Phe113 (blue) are bulky intraportal residues and possible candidate sites for portal mutagenesis to mitigate steric constraints during PQ passage. Met101 and Leu108 were substituted for prolines (yellow), however, the mutants did not grow past 3-5 days after plating. Ala102 (blue) is another site for proline insertion and has not yet been tested.

1.4 Materials and Methods

1.4.1 Growth of Cyanobacterial Cultures

Synechococcus sp. PCC 7002 wild type (ATCC) and mutant strains were grown photoautotrophically in medium A.[13,14] Spectinomycin (100 µg/ml) was added to the growth medium of the mutant. Optimal conditions for growth were 34 °C, incident light intensity of 100-150 µEinstein/m^2/s, and 2% (v/v) CO_2 :air was bubbled into the culture. Cell densities were monitored at 730 nm using a Cary 3 spectrophotometer. The growth curves were fit to an exponential function and the first derivative of these functions in order to compare the growth rate of the mutant and the wild type.

1.4.2 Site-directed Mutagenesis and Plasmid Construction

S. Naurin performed PCR mutagenesis and Jillian Ness performed primer design and aided in plasmid construction. A PCR site-directed mutagenesis method was performed as described.[13,16] Five mutations were introduced via site-directed mutagenesis into a 2.7 kb fragment of *Synechococcus* sp. PCC 7002 genome containing the *petBD* operon: HindIII, P105A, P112A, EcoRV and EcoRI (Table 1.1.). P105A and P112A mutations were added into the petD gene that

encodes subunit IV, changing residues Proline to Alanine at position 105 and 112. The HindIII/EcoRI-HF enzyme-digested PCR product was ligated into HindIII/EcoRI enzyme-digested pUC19 plasmid to make Plasmid I. The construction of the final plasmid used for homolgous transformation is outline in Figure 1.6. Plasmid I was linearized with EcoRV-HF enzyme. The *aadA* cassette was excised from pet423 using SmaI/EcoRV and ligated into plasmid I to make the final construct, plasmid II. This was the final plasmid used to transform the *Synechococcus* cells. Plasmids I and II were transformed in DH5-alpha *E. Coli* cells.[17] Mutations in the *petDB* operon were validated by DNA sequencing prior to transformation into *Synechococcus* PC 7002.

Table 1.1. *Sequences of primers used for PCR site-directed mutagenesis in petD gene and 1 kb flanking sequences in Synechococcus sp. PCC 7002 genome.* Underlined text indicates mutation site. 'Fwd' indicates forward primer; 'Rev' indicates reverse primer.

PetFwdHindIII	5'-GAAAAAGCTTGGGTTTTGAGGGGC-3'
PetRevEcoR1	5'-GAAAGAATTCAAATCGCCAACCAGGATG-3'
PetDFwdEcoRV	5'-CGGCTAAACGATATCGATCGCCTTTTTTG-3'
PetDRevEcoRV	5'-CAAAAAAGGCGATCGATATCGTTTAGCCG-3'
PetDFwdP105/112A	5'-GGGGCGATTGCGTTGGGTTTGATGATGGTGGCTTTCATT-3'
PetDRevP105/112A	5'-AATGAAAGCCACCATCATCAAACCCAACGCAATCGCCCC-3'
PetDFwdM101P	5'-GGTATTGCTTGTCCTGGGCGATT-3'
PetDRevL101P	5-'AATCGCCCCAGGACAAGCAATACC-3'
PetDFwdQ108P	5'-GTTGGGTCCCATGATGGTGCCTTTCATTG-3'
PetDRevQ108P	5'-GAAAGGCACCATCATGGGACCCAACGG-3'

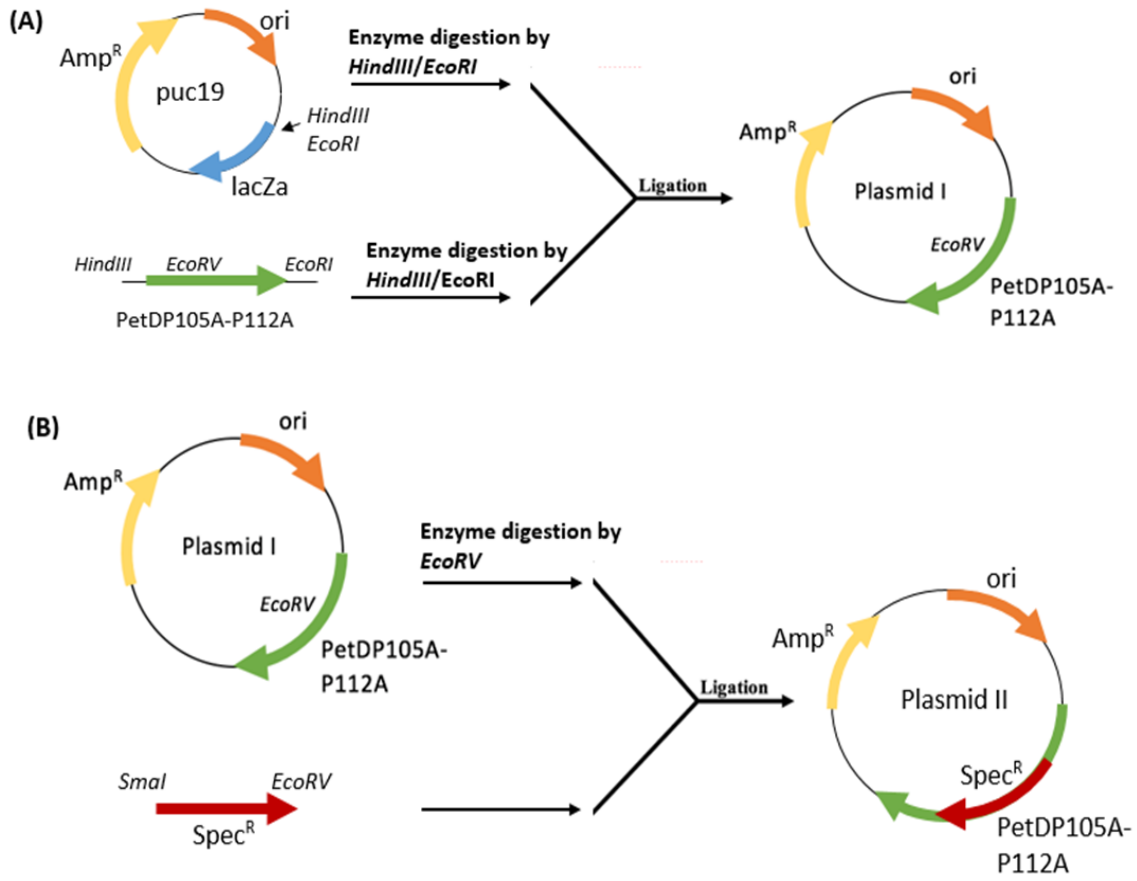

Figure 1.7. *Schematic illustration of plasmid construction.* (A) Construction of Plasmid I through EcoRI, HindIII DNA nuclease digestion of pUC19 and petDP105A-P112A PCR product (contains petD and 5' and 3' 1 kb flanking regions, with a final 2.7 kb PCR product. Digested products are ligated and the plasmid amplified in *E. coli*. (B) Construction of Plasmid II through digestion of SpecR and Plasmid I with blunt DNA nuclease EcoRV and/or SmaI. Digested products are ligated and the plasmid amplified in *E. coli.*

1.4.3 Homologous Transformation of *Synechococcus* and Screening of Mutants

Sejuti Naurin performed homologous transformation, aided by Jillian Ness. Transformation of *Synechococcus* PCC 7002 was performed as described.[6,35] The mixture of plasmid II and cells were incubated at 37 °C under 50-70 µEinsteins/m^2/s of white light for 90 min. The plasmid/cell mixture was then plated on medium A agar containing 100 µg/ml spectinomycin. After 7–10 days of incubation at 37°C under 100 µEinsteins/m^2/s illumination, spectinomycin-resistant transformants were streaked again on spectinomycin-containing plates for further segregation. Segregants with *petD* gene mutations in the *Synechococcus* genome were confirmed by sequencing the PCR fragment.

1.4.4 Flash Kinetic Spectroscopy and Assay of Rate-Limiting Step

The msec reduction rate of cytochrome *f*, assayed by a positive absorbance change in the α-band at 556 nm following photo-oxidation triggered by a light flash (Figure 1.5), is associated with the rate-limiting step of the electron transport chain. Alteration of the 'F' helix by site-directed mutation through removal of 2 Pro residues (Figure 1.1B, C) is predicted to cause a conformation change that reduces the size of the quinone portal and thereby decreases the rate of reduction of cytochrome *f*. The application of the Xenon flash-triggered spectrometer used in these studies on the kinetics of cytochrome turnover in intact algae (*C.reinhardtii*) and cyanobacteria (*Synecococcus*) has been described previously.[23] The electron transfer activity of the cytochrome b_6 *f* complex *in vivo* was measured with respect to the flash-induced oxidation of cytochromes *f* and c_6 in their α-band absorption region with 540 nm as a reference wavelength ($\Delta A_{556\text{-}540\ nm}$) using a triggered Xenon-flash single beam spectrometer as described.[23] *Synechococcus* was harvested in the late-log phase (10 μM chlorophyll) in a medium consisting of 5 mM HEPES (pH 7.5), 10 mM NaCl, 10 mM $NaHCO_3$, 10 μM 3-(3,4-dichlorophenyl)-1,1-dimethylurea (DCMU), 1 mM NH_2OH, and 10 μM carbonyl cyanide *p*-trifluoromethoxy-phenylhydrazone (FCCP). FCCP was added to dissipate the trans-membrane electrochemical potential, and KCN (0.1 mM) to prevent draining of the quinone pool by respiration. Background noise correction: to minimize noise, principally 60 Hz background, in the spectrometer output signal, the output signal was referenced to the pre-flash output function, recording of the absorbance change initiated 0.5 msec after the excitation flash pulse, and the noise suppression algorithm[32] applied to processing of the output signal.

1.5 References

1. Zhu, X.G., Long, S. P., & Ort, D. R. Improving photosynthetic efficiency for greater yield. *Annu Rev Plant Biol* 61:235-261 (2010).

2. Wu, A., Hammer, G. L., Doherty, A. von Caemmerer, S., & Farquhar, G. D. Quantifying impacts of enhancing photosynthesis on crop yield. *Nature Plant* 5: 380-388 (2019).

3. Cramer, W. A., Zhang, H., Yan, J., Kurisu, G., & J. L. Smith. Trans-membrane traffic in the cytochrome b_6f complex. *Ann. Rev. Biochem*., **75**: 769-790 (2006). PMID: 16756511.

4. Hasan, S. S. & Cramer W. A. Internal lipid architecture of the hetero-oligomeric cytochrome b_6f complex. *Structure* **22**:1008-1015 (2014).

5. Cramer, W. A. & Hasan, S S. *The Cytochrome b_6f Lipoprotein Complex*; pp. 177-207 in "*Cytochrome Complexes: Evolution, Structures, Energy Transduction, and Signaling,*" Eds. Govindjee and T. Sharkey (Springer, Dordrecht), volume **41** in the Series "Advances in Photosynthesis and Respiration," eds. Govindjee and T. Sharkey" (Springer, Dordrecht). ISSN 1572-0233; ISBN 978-94-017-7479-6; DOI 10.1007/978-94-017-7481-9 (2016).
6. Hasan S. S. & Cramer W. A. On rate limitations of electron transfer in the photosynthetic cytochrome b_6f complex. *Phys Chem Chem Phys* **14**: 13853-13860 (2012).
7. Blankenship R. E. *et al*. Comparing photosynthetic and photovoltaic efficiencies and recognizing the potential for improvement. *Science* **332**: 805–809 (2011).
8. Nürnberg D-J. *et al*. Photochemistry beyond the red limit in chlorophyll *f*-containing photosystems. *Science* **360**: 1210-1213 (2018).
9. Sukenik, A., Bennett, J., & Falkowski, P. Light saturated photosynthesis-limitation by electron transport or carbon fixation. *Biochim Biophys Acta* **891**: 203-215 (1987).
10. South, P. F., Cavanaugh, A-P, Liu & H-W, Ort D-R. Synthetic glycolate metabolic pathways stimulate growth and productivity in the field. *Science* **263**, 1-9 (2019).
11. Avron, M. & Chance, B. Relation of phosphorylation to electron transport in isolated chloroplasts. *Brookhaven Symp Biol* **19,**149-160 (1966).
12. Stiehl, H.H. & Witt H.T. Quantitative treatment of the function of plastoquinone in photosynthesis. *Z Naturforsch* B, **24**,1588-98 (1969).
13. Böhme, H. & Cramer W. A. Localization of a site of energy coupling between plastoquinone and cytochrome *f* in the electron transport chain of spinach chloroplasts. *Biochemistry* **11**,1155-1160 (1972).
14. Hirano, M., Satoh, K. & Katoh S. Plastoquinone as a common link between photosynthesis and respirsation in a blue-green alga. *Photosyn Res* **1**, 149-162 (1980).
15. Haehnel, W & Trebst, A. Localization of electron transport inhibition in plastoquinone reactions. *J Bioenerg Biomembranes* **14**, 181-190 (1982).
16. Lam, E. & Malkin, R. Reconstruction of the chloroplast noncyclic electron transport pathway from water to NADP with three integral protein complexes. *Proc Natl Acad Sci U. S. A.* **79**, 5494-5498 (1982).
17. Cramer, W.A. *et al*. Some new structural aspects and old controversies concerning the cytochrome b_6f complex of oxygenic photosynthesis. *Ann Rev Plant Physiol* **47**, 477-508 (1996).
18. Yan, J. & Cramer, W. A. Functional Insensitivity of the cytochrome b_6f complex to structure changes in the hinge region of the Rieske iron-sulfur protein. *J Biol. Chem.* **278**, 20925-20933 (2003).
19. Finazzi, G., Buschlen, S., de Vitry, C., Rapaport, F., Joliot, P., & Wollman, F. A. Function-directed mutagenesis of the cytochrome b_6f complex in *Chlamydomonas reinhardtii*. Involvement of the cd loop of cytochrome b_6 in quinol binding to the Qo site. *Biochemistry* **36**, 2867-2874 (1997).
20. Soriano, G.M., Ponamarev, M.V., Piskorowski, R. & Cramer, W. A. Identification of the basic residues of cytochrome *f* responsible for the electrostatic docking interaction *in vitro*: relevance to the electron transfer reaction *in vivo*. *Biochemistry* **3,** 15120-15128 (1998).
21. Martinez, S.E., Huang, D., Szczepaniak, A., Cramer, W.A. & Smith, J.L. Crystal structure of chloroplast cytochrome *f* reveals a novel cytochrome fold and unexpected heme ligation. *Structure* **2**: 95-105 (1994).

22. Zhang, H. *et al*. Characterization and crystallization of the lumen side domain of the chloroplast Rieske iron-sulfur protein. *J Biol Chem* **271**, 31360-31366 (1996).
23. Kurisu, G., Zhang, H., Smith, J.L., & Cramer, W. A. Structure of the cytochrome b_6f complex of oxygenic photosynthesis: tuning the cavity. *Science* **302**, 1009-1014 (2003).
24. Stroebel, D.Y., Choquet, J., Popot, L., & Picot, D. An atypical haem in the cytochrome b(6)f complex. *Nature* **426**, 413-418 (2003).
25. Yamashita. E., Zhang, H., & Cramer, W. A. Structure of the cytochrome b_6f complex: quinone analogue inhibitors as ligands of heme c_n. *J. Mol. Biol.* **370**, 39-52 (2007).
26. Hasan, S.S. & Cramer, W.A. Internal lipid architecture of the hetero-oligomeric cytochrome b_6f complex. *Structure* **22**,1008-1015 (2014).
27. Agarwal R, *et al*., Role of domain swapping in the hetero-oligomeric cytochrome b_6f lipoprotein complex. *Biochemistry* **54**: 3151-63 (2015)
28. Crofts, A.R. *et al*. Pathways for proton release during ubihydroquinone oxidation by the bc_1 complex. *Proc. Natl. Acad. Sci., U. S. A*. **96**, 10021-10026 (1999).
29. Hasan, S.S., Proctor, E.A., Yamashita, E., Dokholyan, N. V. & Cramer, W. A. Traffic within the cytochrome b_6f lipoprotein complex: gating of the quinone portal. *Biophys J* **107**:1620-28 (2014).
30. Cao, Z., and Bowie, J. U. Shifting hydrogen bonds may produce flexible transmembrane helices. *Proc. Natl. Acad. Sci., U. S. A.* **109**, 8121-8126 (2012).
31. Sievers, F. *et al*. Fast, scalable generation of high-quality protein multiple sequence alignments using Clustal Omega. *Mol Syst Biol* 7, report 539 (2011).
32. Marquandt, D.W. Algorithm for Least Squares Estimation of Non-linear Parameters. *J Soc Industrial & Applied Mathematics*, **11**:431-441 (1963).
33. Furbacher, P. N., Girvin, M. E., and Cramer, W. A. (1989) On the question of interheme electron transfer in the chloroplast b_6 *in situ*. Biochemistry, **28**: 8990-8998 (1989).
34. Daniell, H. & Khan M-S. Milestones in chloroplast genetic engineering: an environmentally friendly era in biotechnology. *Trends Plant Sci* 7:84-91 (2002)
35. Buzby, J.S., Porter, R.D. & Stevens, S.E. Expression of the *Escherichia coli* lacZ gene on a plasmid vector in a cyanobacterium. *Science* 230:805-807 (1985).

CHAPTER 2. PGRL1 INTERACTION WITH THE CYTOCHROME b_6f COMPLEX INVOLVED IN CYCLIC ELECTRON TRANSPORT

2.1 Introduction

Linear and photosystem I-centric cyclic photosynthetic electron transport establish a trans-thylakoid proton motive force, comprised of proton gradient (ΔpH) and electrical potential (ΔΨ), to synthesize ATP. The ΔpH gradient induces non-photochemical quenching (NPQ) through lumen acidification in order to dissipate excess excitation energy from the light-harvesting complexes of PSII to keep the plastoquinone pool (Q_p pool) optimally oxidized[1]. In addition, ΔpH is thought to downregulate oxidation of PQH_2 at the Q_o site of the cytochrome b_6f complex, through a process known as 'photosynthetic control.' The PGRL1/PGR5-dependent cyclic electron transport pathway is shown to be essential in establishing these regulations to prevent over-reduction of Fe-S centers on the PSI acceptor side and subsequent superoxide core damage[1].

Cyclic electron transport (CET) contributes to transmembrane ΔpH formation, initiating NPQ feedback inhibition of PSII, thereby shifting the rate-limitation from PSI acceptors to the b_6f complex.[2, 3, 4] The significant contributions of CET in cyanobacteria, algae and in C4 plants are well-studied.[5,6,7] The importance of CET in C3 plants has been characterized only in the last 20 years, shown to be especially significant in stress conditions.[2,8,9]

In order for the light reactions to meet the stoichiometric requirements of the Calvin cycle (2 NADPH/3 ATP at ~200 ppm of CO_2), Allen *et al*. (2003)[10] calculates that CET would have to recycle one electron for every nine that are transferred via the linear electron transport pathway. Given a steady-state flow of 150 $e^- s^{-1}$ and a c-subunit stoichiometry of 13-15 protons per 3 ATP, the cyclic pathway rate would be 16-18 $e^- s^{-1}$, or contribute about 10% to the trans-membrane electrochemical potential gradient. (assuming the Q-cycle in both pathways is constant). Alric *et al.* (2010)[11] confirmed this cyclic rate in *C. reinhardtti* through PSII inhibition, measuring the CET contribution to be 10-15 $e^- s^{-1}$.

In contrast to oxygenic linear electron transport in which there is net accumulation of NADPH, the two primary cyclic pathways proposed for injection of electrons into the main chain are thought to be NAD(P)H-dehydrogenase (NDH)- and PGRL1/PGR5-dependent.[12] The CET pathways recycle electrons from NADPH and ferredoxin to produce ATP. In the case of the antimycin-sensitive[13,14] PGR5/PGRL1-dependent pathway (Proton Gradient Regulation 5; Proton

Gradient Regulation-Like 1), ferredoxin (Fd) is thought to be oxidized by a putative Fd-dependent plastoquinol reductase (FQR) to reduce the b_6f complex via the PQ pool, however the existence of this FQR is yet to be confirmed (Figure 2.1). CET effectively contributes to the pH gradient (ATP synthesis) and alters the redox poise of PSI electron acceptors to donors. The proposed mechanisms of PGRL1-dependent regulation of the ETC will be described in more detail later.

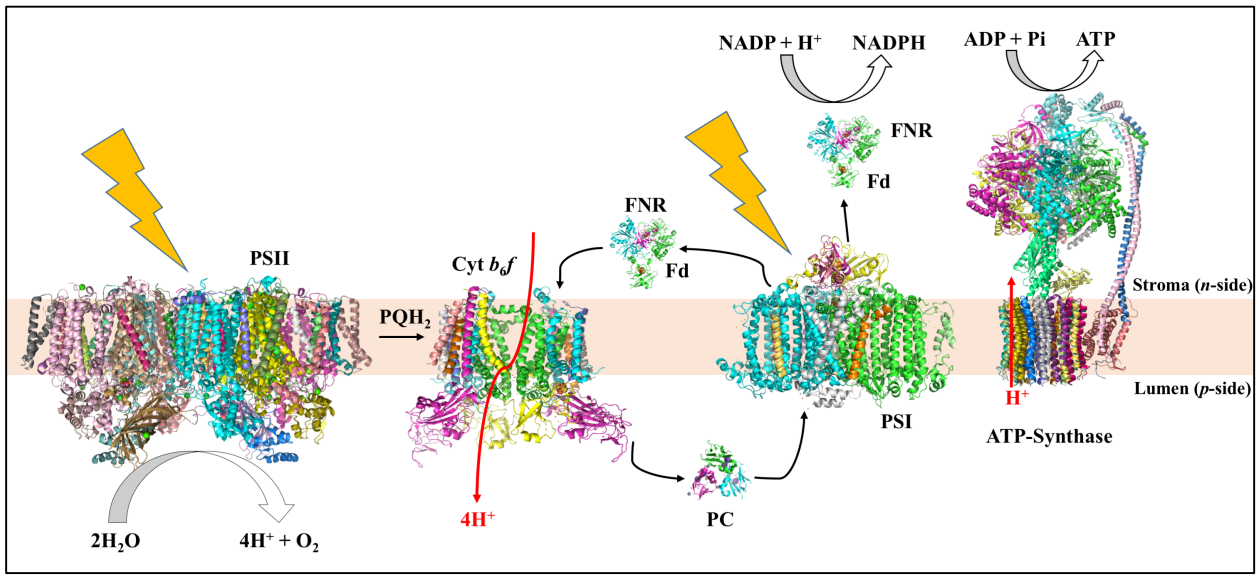

Figure 2.1. *Schematic of linear electron transport* (H2O -> NADP+) *and the PSI-centric Fd-dependent cyclic electron transport pathway of photosynthesis.* Both pathways are thought to contribute to the transmembrane electrochemical potential to be used to produce the proton motive force that drives the synthesis of ATP (ATP Synthase, pdb 6L7P). Linear electron transport (green arrows) (H2O -> NADP+) of oxygenic photosynthesis is mediated by 3 large (0.25-1 MDa) hetero-oligomeric lipoprotein complexes PSII (pdb 5XNL), cyt b_6f (pdb 2E74) and PSI (pdb 6IGZ). The PGRL1/PGR5 pathway of cyclic electron transfer (backward arrow) is thought to recycle electrons from PSI electron acceptor FNR and high-affinity bound Fd to the cyt b6f to contribute to the electrochemical gradient used to synthesize ATP. This is thought to be done through (i) an undiscovered FQR that oxidizes FNR-Fd bound complex to reduce the PQ pool or, (ii) Fd directly reducing the Q_i site hemes of cyt b_6f in a noncononical Q-cycle. PGRL1 and PGR5 proteins' role is thought to be necessary, but mechanistically unknown in this cycle.

The partial redundancy of the two CET pathways was first observed in tobacco, in which there was no detectable difference in phenotype between wild type and an NDH mutant; however, when antimycin A was introduced to attenuate the PGRL1/PGR5 pathway, there was a 30% decrease in CO_2 assimilation and fluorescence of PSII, both indicators of the rate of photosynthesis.[13,14] The PGR5 protein was first characterized as a small, thylakoid protein in *Arabidopsis thaliana*, where it was implicated in its contribution to NPQ within the PSII antenna and photosynthetic control at the cytochrome b_6f level during dark-to-light transitions, conditions of high light intensity, and low CO_2 availability in knockout studies.[15, 16, 17, 18,19]

PGRL1 (Proton Gradient Regulatory-Like 1) is a thylakoid integral membrane protein found to form a ~71 kDa homodimer, as well as a heterodimer with PGR5. PGRL1 mutants are shown to be just as deleterious to photosynthetic efficiency as *pgr5* in *Arabidopsis.*[20,21] PGRL1 was necessary for recruitment of PGR5 to the thylakoid membrane, as PGRL1 mutant thylakoid fractions do not contain detectable amounts of PGR5.[20]

Stoichiometric values of thylakoid proteins from *Arabidopsis* indicate there are 10 PSI to 6 cyt b_6f, with the sub-stoichiometric cyt b_6f potentially serving as a checkpoint to prevent over-reduction of PSI by placing the rate-limitation on cyt b_6f-mediated electron shuttling. The cyt b_6f to PGRL1 ratio is shown to be 5:1 and cyt b_6f to PGR5 to be 1:12.[23] The relative low stoichiometry of PGRL1-dependent pathway proteins is surprising in the face of knockout PGR protein strains showing a 30-40% decrease in functional PSI and electron transport rate in light conditions greater than ~180 μmol photons m^{-2} s^{-1}.[14, 16, 18] Although the PGRL1 thylakoid concentration showed to be five times that of NDH, the NADH electron acceptor in an alternate CET pathway.

The cumulative literature on the PGRL1-dependent cycle in angiosperms characterizes it as a protective mechanism against PSI over-reduction and subsequent time-costly core damage.[24,25] The current hypotheses of the PGRL1 role in CET are as follows: (i) DalCoroso *et al*. (2008)[20] proposes PGRL1 must be important in the formation of a supercomplex between cyt b_6f and PSI in the switch from LET to CET in the nonappresed regions of thylakoids based on two-hybrid yeast assays showing PGRL1 interactions with CET proteins.

(ii) Mosebach *et al*. (2017)[26] purposes PGRL1 aids indirectly/directly in the recruitment of (Fd)-NADP(H) oxioreductase (FNR) to PSI and/or b_6f based on the observation that FNR presence in the thylakoid membranes is attenuated in the absence of PGR5. They extend upon their hypothesis in Buchert *et al*. (2019)[27] suggesting that the cyt b_6f acts as the FQR, where PGRL1/PGR5 aids in the reduction of heme c_n. The PGR5 mutant shows a slower b-heme oxidation rate in the cytochrome b_6f complex in *C. reinhardtii*, therefore they hypothesize that Fd is the electron donor to heme c_n to promote Q.cycle efficiency. This Fd-assisted Q-cycle mode is initiated by PGRL1/PGR5, competing for Fd with linear electron transport.

(iii) Nawrocki *et al.* (2019)[28] measures maximal CET rates in a PGRL1 knockout strain relative to wild type in the algae, *C. reinhardtii.* To overcome electron-limitations due to ETC oxidation, they modulate PSI electron donors during PSII inhibition. In these experiments, PGRL1 mutant and wild type *C. reinhardtii* strains had no significant difference in maximal CET rates, only

shortened PGRL1 mutant maximal rates. They conclude that PGRL1 is not the putative FQR, but that PGRL1 could aid in the regulation of CET duration.

Rantala *et al*. (2020)[29] results support Nawrocki *et al.* (2019)[28] finding that PGRL1 does not have the robust electron-accepting capacitance that the PSI-protective flavodiron system in the moss *Physcomitrella patens.* Flavodiron's direct electron acceptance, unlike PGRL1/PGR5, makes it resistant to photoinhibition[30]. Instead, they found that PGRL1/PGR5 systems are upregulated in conditions of PSI photoinhibition to facilitate the pH-dependent regulation of PSII to PSI electron transport.

There is no agreed function of PGRL1 that can be distilled from the *in vivo* studies probing its role in CET. It is necessary to identify PGRL1's binding partners to begin to understand its mechanistic or regulatory role in CET. The few proposed binding partners come from evidence of a cytochrome b_6f complex and PSI/LHCI/LHCII supercomplex, where they suggest PGRL1 and FNR would bind in the switch from linear to cyclic electron transfer.[31]

In the present study, a biochemical approach is taken to characterize the thermodynamic binding parameters between *Arabidopsis thaliana* PGRL1 and the cytochrome b_6f complex using isothermal titration calorimetry (ITC) to give insight into the role of PGRL1 in the cyclic electron transport chain of photosynthesis.

2.2 Results and Discussion

2.2.1 Results

Truncated His-tagged PGRL1 from Arabidopsis thaliana was cloned and expressed in *E. Coli* and purified according to Hertle *et al.* (2013)[21]. The purified PGRL1 was verified through mass spectroscopic analysis (Proteomics Facility, Purdue University). The dimeric cytochrome b_6f complex was purified from *Arabidopsis thaliana* and spinach according to Baniulis *et al*. (2011)[32] (Figure 2.2A).

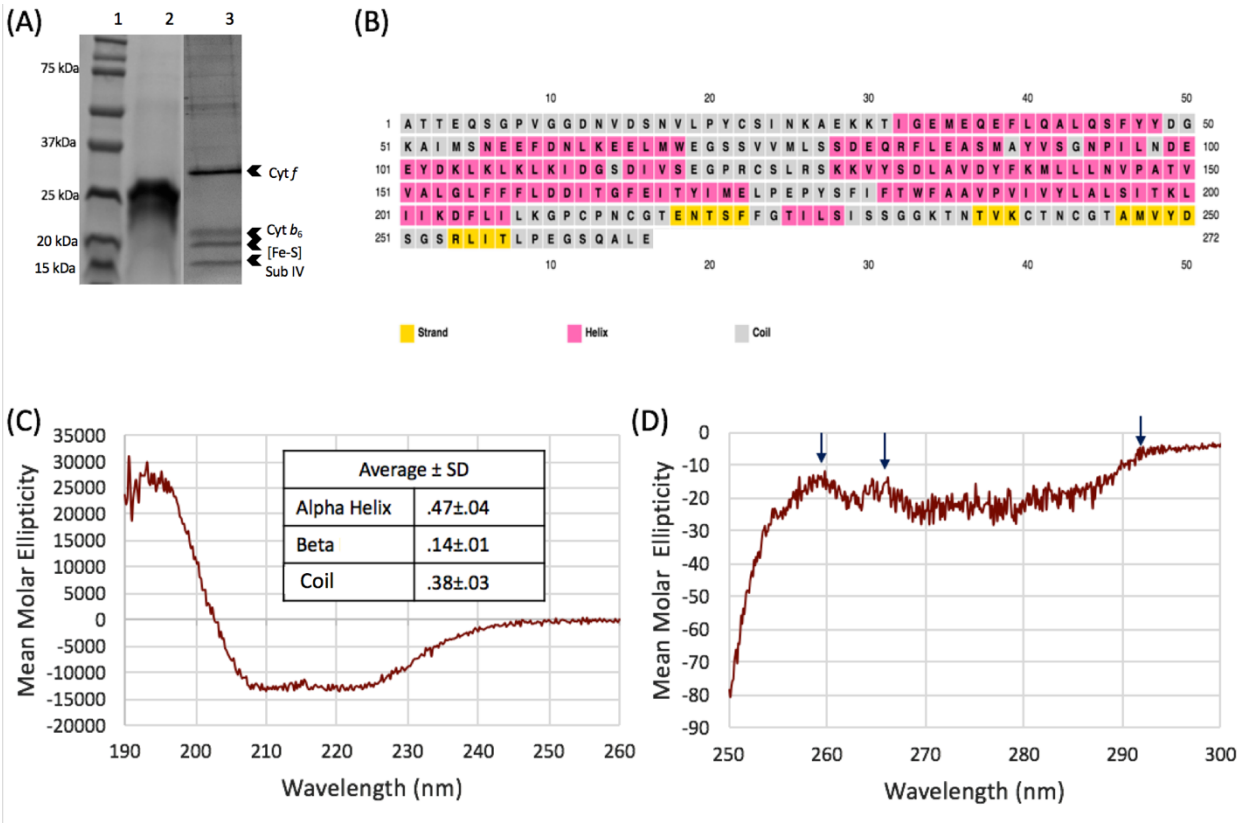

Figure 2.2 *Protein purification and circular dichroism spectroscopy measurements.* **(A)** 12% SDS-PAGE gel showing purified recombinant 30 kDa truncated His-PGRL1(lane 2) and the cytochrome b_6f complex (lane 3); purified as described in methods and materials. **(B)** PSIPRED secondary structure profile of truncated PGRL1 protein sequence. Yellow signifies beta strand, pink as alpha helical and grey as coil. **(C)** Circular dichroism spectra of PGRL1 measured in the far-UV (190-260 nm). The inset shows the average secondary structure content calculated from the CD spectrum (alpha helix, beta strand, and coil) using programs SELCON3, CONTIN, CDSSTR and, K2D.[33] The spectrum, an average of five trials, was measured using 0.1 nm increments with a 0.02 mm cuvette **(D)** Circular Dichroism spectra of PGRL1 measured in the near-UV (250-320 nm) captures the fluorescence of aromatic residues in a hydrophobic environment. The broad peak at 291 belongs to Trp, while the peaks below 270 nm are bands of Phe and Tyr. The spectrum, an average of 20 trials, was measured using .4 nm increments in a 1 cm cuvette. All CD experiments performed in 10 mM HEPES [pH 7.5], .06% (w/v) DDM with a PGRL1 concentration of 4 mg/ml.

To identify the secondary structure composition and presence of tertiary structure of the purified PGRL1, far-UV and near-UV circular dichroism spectra were employed. Although no structure analysis has been done on the PGRL1 membrane protein, the secondary structure prediction program, PSIPRED (PSI-Blast Based Secondary Structure PREDiction), was used as a reference to compare the CD result. PSIPRED uses PSI-BLAST (Position-Specific Iterated BLAST) to find conserved protein sequences of solved proteins to predict the secondary structure of the query. PSIPRED predicts PGRL1 to have approximately ~50% alpha helical content with at least two greater than 20 amino acid runs that appear to be membrane spanning domains (Figure 2.2A). The inset of Figure 2.2C displays the average and standard deviation of the programs used

to estimate the secondary structure from the far-UV PGRL1 CD spectrum. Far-UV CD (190-260 nm) scans revealed the truncated PGRL1 to contain about 47% alpha helix and 15% beta barrel structures. In order to discern the presence of a folded, tertiary structure, near-UV spectra were measured of PGRL1 (Figure 2.2D). Near-UV (250-320 nm) CD signal of aromatic residues occurs only when the residues are embedded in a hydrophobic envrionment. The broad peak at 291 is a band for Trp, while the peaks less than 270 nm are bands of Phe and Tyr, all evidence of a folded PGRL1 protein.

In vivo studies have been performed to show the impact of PGRL1 knockouts on electron transfer in CET, however, the hypotheses of the PGRL1 mechanistic involvement need to be verified through biophysical analyses of PGRL1 binding partners. In this study, isothermal titration calorimetry (ITC) experiments are performed to measure PGRL1 and cytochrome b_6f complex binding to understand if PGRL1 binds to modulate LET mode to CET mode.

In the ITC experiments, purified PGRL1 was titrated into *Arabadopsis thaliana* or *Spinacea oleracea* cytochrome b_6f complex in 10 mM HEPES to measure the binding thermodynamics of this interaction (Figure 2.3A). The upper panels show the raw data of the titration (μcal/sec) and the lower panels show the integrated raw data after subtracting the heat of ligand dilution into buffer (kcal/mol). Of these experiments, there was not a detectable interaction of PGRL1 with the cyt b_6f complex, with the greatest average change in enthalpy, 1.6 kcal/mol, occurring at the 10 °C conditions (Table 2.1). This endothermic enthalpy change indicates a possible displacement of ordered waters, although these conditions do not show evidence of a significant interaction in which binding parameters can be obtained.

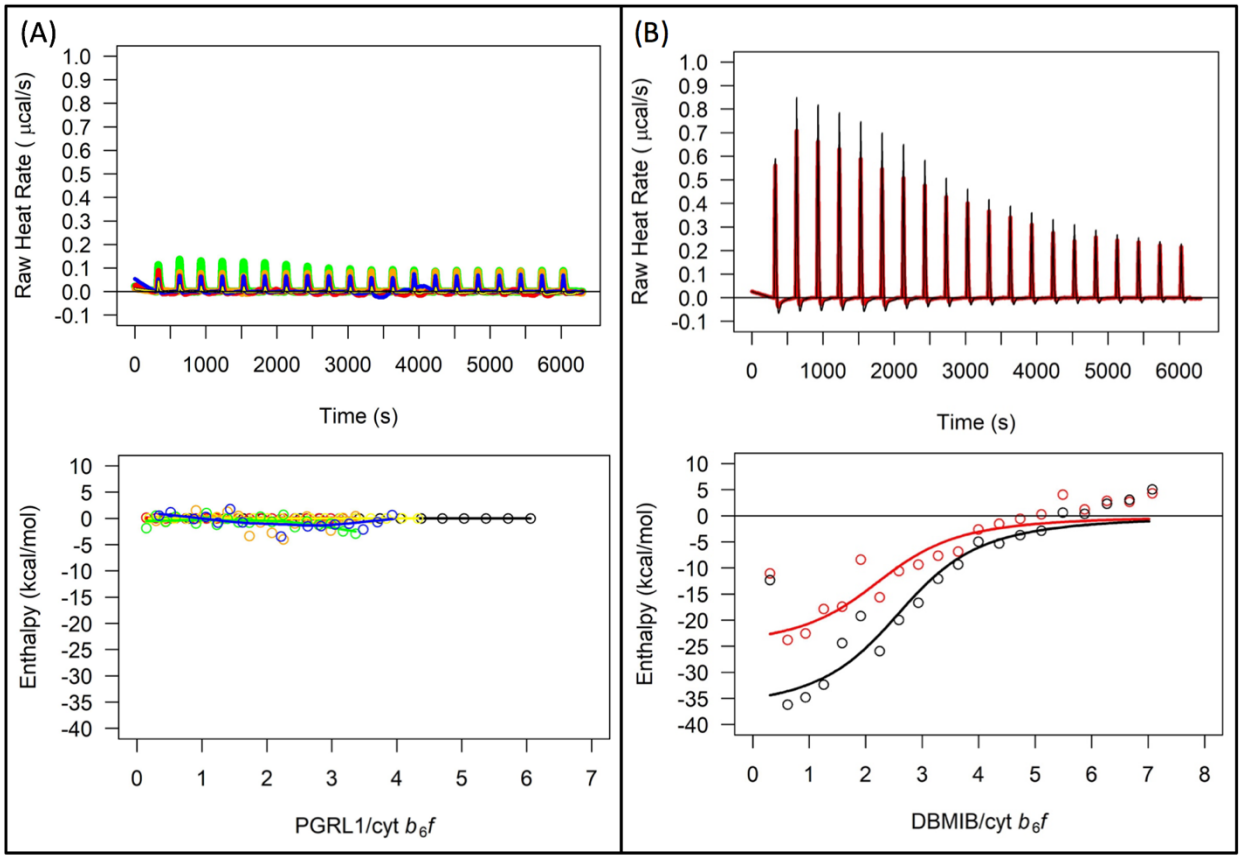

Figure 2.3. *Isothermal titration calorimetry (ITC) profiles monitoring the binding thermodynamics PGRL1 to spinach cyt b b_6f and Arabidopsis cyt b_6f to DBMIB, a quinone analog inhibitor at 20 °C and 10 °C.*[34] All binding parameters were calculated from the fit model using NanoAnalyze.[35] The **upper panels** show the raw data of the titration (μcal/sec) and the **lower panels** show the integrated raw data after subtracting the heat of ligand dilution into buffer (kcal/mol). The first point of the integration curve was excluded, as per convention. Raw heat rates of ligand to buffer controls shown in supplementary Fig. 2.4. **(A)** ITC traces of PGRL1 and the cytochrome b_6f complex in six different conditions fit with best fit models. The following conditions were tested for PGRL1 and *A. thaliana* b_6f in 10 mM HEPES [pH 7.5], 50 mM NaCl and .06% (w/v) UDM: (1) 5 mM BME at at 10°C; [b6f dimer]=7 μM; [PGRL1]= 200 μM at 10°C (trials=2; black trace) (2) 5 mM BME at 20 °C; [b6f dimer]=5 μM; [PGRL1]= 115 μM (trials=1; yellow). Spinach b_6f was used for the subsequent experiments, as subunit cyt b_6 and subunit IV protein sequences are 99% conserved between spinach (UniProtKB P00165/P00166) and A. thaliana (PBMID 10574454). The next experiments were done in 50 mM NaCl and .06% (w/v) DDM with: (3) 10 mM HEPES [pH 7.5], 10 mM BME at 20 °C; [b6f dimer]=5 μM; [PGRL1]= 90 μM (trials=2; green), (4) 10 mM HEPES [pH 6.8], 10 mM BME at 10°C; [b6f dimer]=5 μM M; [PGRL1]=90 μM M (trials=2; orange), (5) 10 mM HEPES [pH 7.5], 100mM NaCl, 5 mM BME at 10°C; [b6f dimer]=5 μM; [PGRL1]= 70 μM (trials=1; blue), (6) 20 mM sodium phosphate buffer [pH 7.5], at 10 °C; [b6f]=5 μM; [PGRL1]= 70 μM (trials=1; red). **(B)** ITC of cyt b_6f and DBMIB in 10 mM HEPES [pH 7.5], 50 mM NaCl, .06% DDM (w/v) [b6f dimer]=7 μM and [DBMIB]= 200 μM at 10 °C (black trace) and 20 °C (red trace). Traces fit with an independent binding model using NanoAnalyze.[35]

As a confirmation of the dimeric b_6f complex binding ability in these buffer conditions and temperatures, the quinone analog inhibitor, DBMIB, was used as a b_6f ligand control. DBMIB contains a binding site at the Q_p pocket of each b_6f complex monomer on the p-side, with greater than one DBMIB able to bind per pocket.[37] This is approximately where a cyclic electron cofactor

would bind if it were to reduce plastoquinone or shuttle FNR in cyclic electron transfer as purposed of PGRL1.[21, 27] The DBMIB/cyt b_6f ITC experiment was performed in the presence of 10 mM HEPES, 50 mM NaCl, .06% (w/v) DDM [pH 7.5] at 10°C (black trace) and 20 °C (red trace) (Figure 2.3B). These experiments show similar enthalpy-driven, exothermic binding reactions, with an average K_d of $3.85x10^{-6}$ M, binding ratio of 2.4, or approximately one DBMIB/ b_6f monomer, ΔG of -7.1 kcal/mol, ΔH of -6.2 kcal/mol, and an average ΔS of -.74 cal/mol•K (Table 2.1). Because of the difference in temperatures, there is a difference in the temperature-dependent enthalpy component between the two conditions by 1 kcal/mol. The exothermic nature of this binding interaction is not surprising, as the bromide substituents of the DBMIB inhibitor are proposed to form a hydrogen bridge with the histidines coordinating the [Fe-S] cluster.[37]

Table 2.1.*Thermodynamic parameters obtained by isothermal titration calorimetry* for the binding of cyt b_6f and the quinol analog, DBMIB at 10 °C (trials=1) and 20 °C (trials=1) and cyt b_6f and PGRL1 at 10 °C (trials= 3) and 20 °C (trials=3). An * indicates averaged values.

	T (°C)	K_d E-6 (M)	n	ΔG (kcal · mol^{-1})	ΔH (kcal · mol^{-1})	ΔS (cal · mol^{-1}· K^{-1})
DBMIB/ cyt b_6f complex	10.0	2.5	2.5	-7.2	-7.7	-1.00
	20.0	5.2	2.3	-7.0	-6.7	-0.48
PGRL1/ cyt b_6f complex	10.0	–	–	–	1.6*	–
	20.0	–	–	–	~ 0*	–

2.2.2 Discussion

Only in recent years has cyclic electron transfer shown to be fundamental in the regulation of electron flow for the maximal fitness of plants, cyanobacteria, and algae.[2,5,6,7,8,9] The contribution to ATP synthesis via the transmembrane electrochemical gradient and, during high light intensity, PSII non-photochemical quenching in preventing photoinhibition are thought to be the primary mechanisms in which CET electron transport regulation occurs. The assembly and disassembly of a supercomplex in the switch of electron flow between LET and CET seems to be the most likely mechanism. The literature demonstrates that PGRL1 is necessary for efficient CET: PGRL1 knockout studies indicate PSI oxidation and electrochromic band shift measurements (measurements of cyclic electron transport rate) decrease by 40% relative to wild type, with an

increase in damaged PSI;[20,21,24] however, it is shown that PGRL1 does not participate as a direct electron cofactor in CET between PSI and cyt b_6f.[28,29]

The ITC results from this study provide evidence that PGRL1 and the cytochrome b_6f complex do not directly interact significantly. This result supports Nawrocki et al. (2019)[28] and Rantala *et al*. (2020)[29] data that suggest PGRL1 is *not* a direct electron acceptor that funnels electrons back to the cytochrome b_6f complex to shift LET to CET. The sub-stoichiometric amounts of PGRL1 relative to other LET/CET machinery, FNR, PC, Fd, cyt b_6f, PSI, also support PGRL1's role as a possible regulatory factor in CET rather than an electron conduit for the cytochrome b_6f complex.

2.3 Future Directions

Cyclic electron transfer proves to be essential in the maintenance of the redox poise, preventing photosystem I over-reduction and subsequent damage. The PGRL1 and PGR5 proteins participate in the possible regulation of CET.[15,16,17,18,19] Finding the roles of the elusive PGRL1 and PGR5 proteins is an exciting opportunity in the study of cyclic electron transfer regulation.

In order to confirm there is no interaction between cyt b_6f and PGRL1, further cross-linking studies need to be performed. We performed an *in vitro* cross-linking study between PGRL1 and cytochrome b_6f, however, because of PGRL1's propensity to form homo-multimeric complexes as a result of the six conserved cysteines, antibodies against b_6f are needed to detect possible complexes with PGRL1. It would be useful to further use ITC to detect possible interactions between PGRL1 and known CET proteins: FNR, Fd, Pc, and PSI. It would be useful to perform pull-down assays with PGRL1 (bait PGRL1 attached to column using its N-terminal His-tag) to detect binding partners from thylakoid lysate if PGRL1 proves to not bind to the main CET machinery from ITC and cross-linking.

In addition, PGRL1 does demonstrate electron transfer capacity via two pairs of conserved cysteine groups,[21] but further research needs to be performed to establish the redox potential of PGRL1. Further, although Hertle et al. (2013)[21] shows the metal cofactor of PGRL1 is not needed for electron transfer activity, EPR can still be used to characterize PGRL1's cofactor to provide an insight into its structural or functional purpose.

PGRL1 is shown to form a heterodimer with the soluble PGR5.[20] This is a possible candidate pair to test with ITC, in addition seeing how this dimer interacts with the other CET cofactors. *A.*

thaliana PGR5 cDNA in pet21b was given by the Puthiyaveetil lab at Purdue University, however, upon sequencing and transformation in *E. Coli* cell lines, BL21 (DE3) and Rosetta (DE3), and testing in various expression conditions, PGR5 was not isolated. It could be beneficial to find conditions for PGR5 expression.

2.4 Materials and Methods

2.4.1 Cytochrome b_6f Purification

The cytochrome b_6f complex was isolated from commercially purchased spinach leaves. Spinach b_6f were isolated as described previously;[32] HEPES-HCl was substituted for Tris-HCl in all buffers to utilize its more acidic buffering range. Dimeric and monomeric cyt b_6f complex were separated through sucrose density gradients and size exclusion chromatography. Dimeric b_6f (active form) was used for all biochemical assays.

2.4.2 Recombinant PGRL1 Expression and Purification

The predicted mature recombinant PGRL1 cDNA gene without the chloroplast signaling peptide was inserted into pET21b and introduced into *E. Coli Rosetta* cells; the His_6-tagged PGRL1 cell lines were a gift from I.M. Ibrahim, Department of Biochemistry, Purdue University. The expression and purification procedure of recombinant proteins were based upon Hertle et al. (2013)[21] methods: the strains were grown in YT medium containing 100 μg/ml of ampicillin (Sigma) at 37 °C and induced with .5 mM isopropyl-1-thio-β-D-thiogalactopyranoside (IPTG, Sigma) at A_{600} of 0.5–0.8. In addition, 2 mM $(NH_4)_2Fe(SO_4)_2$ (Sigma) was added upon expression induction. Protein expression was allowed for 3 hours at 30°C wherein the cells were pelleted at 4,000 g and used immediately or stored at -80°C.

All experiments were carried out using buffers O_2 purged overnight with N_2 gas (Purdue General Store). Cells were resuspended in 50 mM NaH_2PO_4, 1% [w/v] n-Dodecyl β-D-maltoside (DDM, Anatrace), 300 mM NaCl, 10 mM imidazole, 1 mM phenylmethylsulfonyl fluoride (PMSF, Sigma), 1 mM DTT (Sigma), 5 μg/ml DNase (Sigma) [pH 7.5]. The suspended cells were run through an Avestin Emulsiflex C3 three times at 1,500 psi for optimal cell lysis (ATA Scientific Instruments). The lysate was centrifuged at 45,000 g for 45 minutes. The supernatant and regenerated nickel-nitriloacetic acid matrix (Ni beads) were combined in a Falcon tube,

wherein the tube was gently spun end over end at 4°C for 60 minutes. The Ni beads were pelleted at 500 g for 10 minutes and the supernatant was poured away and stored to be run on a 12% SDS page gel. The Ni beads were put on a gravity column and washed with 50 mM NaH_2PO_4, 0.06% (w/v) DDM, 300 mM NaCl, 20 mM imidazole (pH 7.5) and eluted with 50 mM NaH_2PO_4, 0.06% (w/v) DDM, 300 mM NaCl, 250 mM imidazole (pH 7.5). The PGRL1- containing fractions were verified with a 12% SDS page gel and mass spectroscopy (Proteomics Facility, Purdue University) Subsequent fractions were verified through A_{280} measurements. The collected fractions were subjected to Superdex 200 size exclusion chromatography using 15 mM HEPES (pH 7.5), .1 M NaCl, and 0.045% UDM or .06% DDM. Purified recombinant protein was used for biochemical analysis, or flash-frozen and stored at -80 °C.

2.4.3 Isothermal Titration Calorimetry Measurements

The Isothermal titration calorimetry (ITC) experiments were performed using a Nano DSC TA Instrument and analyzed using NanoAnalyze software (TA Instruments)[35]. The injection syringe was calibrated initially by mass of water.[36] Data was collected with a constant baseline adjustment to account for stirring enthalpy contribution. The data was integrated from the injection start to 500 s post injection. The first point of integration was excluded, per convention.

All ITC experiments contained the following parameters: the macromolecule volume was 200 µl, the ligand volume 50 µl, the data collection was one point/second, the titration rate was 20 injections of 2.45 µl delivered every 300 seconds using a stir rate of 300 rpm. All ligand dilution heat rates (ligand to buffer) were subtracted from ligand to macromolecule heat rates using the same buffer conditions and ligand concentrations.

ITC experiments with PGRL1 and the cytochrome b_6f complex were performed in six different conditions. The following conditions were tested for PGRL1 and *A. thaliana* b_6f in PGRL1 in 10 mM HEPES [pH 7.5], 50 mM NaCl and .06% (w/v) UDM: (1) 5 mM BME at 10°C; [b6f dimer], 7 μM; [PGRL1], 200 μM at 10°C (trials, 2; black trace) (2) 5 mM BME at 20 °C; [b6f dimer], 5 μM; [PGRL1], 115 μM (trials, 1; yellow). Spinach b_6f was used for the subsequent experiments, as subunit cyt b_6 and subunit IV protein sequences are 99% conserved between spinach (UniProtKB P00165/P00166) and *A. thaliana* (PBMID 10574454). The next experiments were done in 50 mM NaCl and .06% (w/v) DDM with: (3) 10 mM HEPES [pH 7.5], 10 mM BME at 20 °C; [b6f dimer],5 μM; [PGRL1], 90 μM (trials, 2; green), (4) 10 mM HEPES [pH 6.8], 10

mM BME at 10°C; [b6f dimer], 5 μM; [PGRL1], 90 μM (trials, 2; orange), (5) 10 mM HEPES [pH 7.5], 5 mM BME at 10°C; [b6f dimer], 5 μM; [PGRL1], 70 μM (trials, 1; blue), (6) 20 mM sodium phosphate buffer [pH 7.5], at 10 °C; [b6f], 5 μM; [PGRL1], 70 μM (trials, 1; red) (Figure 2.3). Since the sigmoidal curve models were not able to fit the data, best fit curves were fit instead.

ITC of cyt b_6f and DBMIB in 10 mM HEPES [pH 7.5], 50 mM NaCl, .06% DDM (w/v) [b6f dimer], 7 μM and [DBMIB], 200 μM at 10 °C (black trace) and 20 °C (red trace) (Figure 2.3). The integrated data were individually fit with independent binding models.[35]

2.4.4 Circular Dichroism Spectroscopy

CD and simultaneous optical density scans were measured using a spectropolarometer ["Chirascan" (Applied Photophysics Ltd. UK)]. All CD experiments performed in 10 mM HEPES [pH 7.5], .06% DDM with a PGRL1 concentration of 4 mg/ml. Far-UV CD measurements, in the wavelength range of 260-190 nm, were measured using a cell path length of .02 mm with .1 nm increments. Five trials were averaged. The near UV circular dichroism spectrum, an average of 20 trials, was measured using .4 nm incruments in a 1 cm cuvette.

2.5 Supplementary Figure

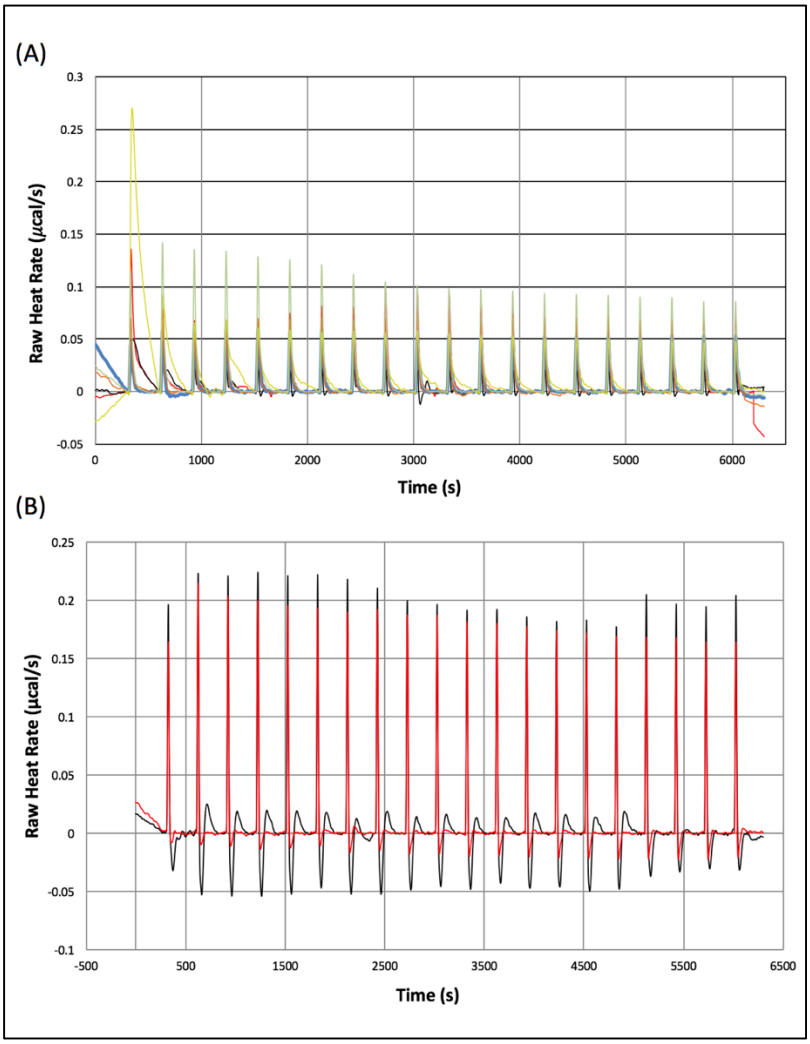

Figure 2.4. ITC trace of the raw heat rate of ligand to buffer control in the same six conditions as Figure 2.3. These controls were used to subtract the ligand dilution heat from the ligand to macromolecule ITC experiments in Figure 2.3. (A) The following conditions were tested for PGRL1 in 10 mM HEPES [pH 7.5], 50 mM NaCl and .06% (w/v) UDM: (1) 5 mM BME at at 10°C; [b6f dimer]=7 μM; [PGRL1]= 200 μM at 10°C (trials=2; black trace) (2) 5 mM BME at 20 °C; [PGRL1]= 115 μM (trials=1; yellow). The next experiments were done in 50 mM NaCl and .06% (w/v) DDM with: (3) 10 mM HEPES [pH 7.5], 10 mM BME at 20 °C; [PGRL1]= 90 μM (trials=2; green), (4) 10 mM HEPES [pH of 6.8], 10 mM BME at 10°C; [b6f dimer]=5 μM; [PGRL1]=90 μM (trials=2; orange), (5) 10 mM HEPES [pH 7.5], 5 mM BME at 10°C; [PGRL1]= 70 μM (trials=1; blue), (6) 20 mM sodium phosphate buffer [pH 7.5] at 10 °C; [PGRL1]= 70 μM (trials=1; red). (B) ITC control of DBMIB to buffer in 10 mM HEPES [pH 7.5], 50 mM NaCl, .06% (w/v) DDM and [DBMIB]= 200 μM at 10 °C (black trace) and 20 °C (red trace).

2.6 References

1. Grieco M, Tikkanen M, Paakkarinen V, Kangasjärvi S, Aro E-M (2012) Steady-State Phosphorylation of Light-Harvesting Complex II Proteins Preserves Photosystem I under Fluctuating White Light. *Plant Physiol* 160(4):1896–910.

2. Joliot P, Joliot A (2002) Cyclic electron transfer in plant leaf. *PNAS* 99(15):10209–14.

3. Kramer DM, Johnson G, Kiirats O, Edwards GE (2004) New Fluorescence Parameters for the Determination of Q_A Redox State and Excitation Energy Fluxes. *Photosynthesis Research*. 79(2):209–18.

4. Chaux F, Peltier G, Johnson X (2015) A security network in PSI photoprotection: regulation of photosynthetic control, NPQ and O2 photoreduction by cyclic electron flow. *Front Plant Sci* 6:1–7

5. Herbert SK, Fork DC, Malkin S (1990) Photoacoustic Measurements *in Vivo* of Energy Storage by Cyclic Electron Flow in Algae and Higher Plants. *Plant Physiol* 94(3):926–34.

6. Asada K, Heber U, Schreiber U (1993) Electron flow to the intersystem chain from stromal components and cyclic electron flow in maize chloroplasts, as detected in intact leaves by monitoring redox change of P700 and chlorophyll fluorescence. *Plant Cell Physiol* 34:39-50.

7. Ravenel J, Peltier G, Havaux M (1994) The cyclic electron pathways around photosystem I in Chlamydomonas reinhardtii as determined in-vivo by photoacoustic measurements of energy storage. *Planta* 193: 251-259.

8. Golding AJ, Finazzi G, Johnson GN (2004) Reduction of the thylakoid electron transport chain by stromal reductants evidence for activation of cyclic electron transport upon dark adaptation or under drought. *Planta* 220(2):356–63.

9. Joliot P, Joliot A (2006) Cyclic electron flow in C3 plants. *BBA – Bioenergetics* 1757(5–6):362–8.

10. Allen JF (2003) Cyclic, pseudocyclic and noncyclic photophosphorylation: new links in the chain. *Trends in Plant Science* 8(1):15–9.

11. Alric J, Lavergne J, Rappaport F (2010) Redox and ATP control of photosynthetic cyclic electron flow in Chlamydomonas reinhardtii (I) aerobic conditions. *BBA – Bioenergetics* 1797(1):44–51.

12. Arnon DI, Allen MB, Whatley FR (1954) Photosynthesis by Isolated Chloroplasts. *Nature* 174(4426):394–6.

13. Genty B Goulas Y Dimon B Peltier G Briantais JM Moya I (1992) Modulation of efficiency of primary conversion in leaves, mechanisms involved at PS2. Research in photosynthesis, Vol. IV: Proceedings of IXth International Congress on Photosynthesis.

14. Joët T, Cournac L, Horvath EM, Medgyesy P, Peltier G (2001) Increased Sensitivity of Photosynthesis to Antimycin A Induced by Inactivation of the Chloroplast *ndhB* Gene. Evidence for a Participation of the NADH-Dehydrogenase Complex to Cyclic Electron Flow around Photosystem I. Plant Physiol 125(4):1919–29.

15. Munekage Y, Hojo M, Meurer J, Endo T, Tasaka M, Shikanai T (2002) PGR5 Is Involved in Cyclic Electron Flow around Photosystem I and Is Essential for Photoprotection in Arabidopsis. Cell 110(3):361–71.

16. Okegawa Y, Long TA, Iwano M, Takayama S, Kobayashi Y, Covert SF, et al (2007) A Balanced PGR5 Level is Required for Chloroplast Development and Optimum Operation of Cyclic Electron Transport Around Photosystem I. Plant and Cell Physiology 48(10):1462–71.

17. Foyer CH, Neukermans J, Queval G, Noctor G, Harbinson J (2012) Photosynthetic control of electron transport and the regulation of gene expression. Journal of Experimental Botany 63(4):1637–61.

18. Suorsa M, Järvi S, Grieco M, Nurmi M, Pietrzykowska M, Rantala M, et al (2012) PROTON GRADIENT REGULATION5 Is Essential for Proper Acclimation of *Arabidopsis* Photosystem I to Naturally and Artificially Fluctuating Light Conditions. *Plant Cell* 24(7):2934–48.

19. Yamori W, Makino A, Shikanai T (2016) A physiological role of cyclic electron transport around photosystem I in sustaining photosynthesis under fluctuating light in rice. *Sci Rep* 6(1):20147.

20. DalCorso G, Pesaresi P, Masiero S, Aseeva E, Schünemann D, Finazzi G, et al (2008) A Complex Containing PGRL1 and PGR5 Is Involved in the Switch between Linear and Cyclic Electron Flow in Arabidopsis. *Cell* 132(2):273–85.

21. Hertle AP, Blunder T, Wunder T, Pesaresi P, Pribil M, Armbruster U, et al (2013) PGRL1 Is the Elusive Ferredoxin-Plastoquinone Reductase in Photosynthetic Cyclic Electron Flow. *Molecular Cell* 49(3):511–23.

22. Brzezowski, P., Ksas, B., Havaux, M. *et al* (2019) The function of PROTOPORPHYRINOGEN IX OXIDASE in chlorophyll biosynthesis requires oxidised plastoquinone in *Chlamydomonas reinhardtii*. *Commun Biol* 2**:** 159.

23. McKenzie SD, Ibrahim IM, Aryal UK, Puthiyaveetil S (2020) Stoichiometry of protein complexes in plant photosynthetic membranes. *Biochim Biophys Acta Bioenerg* 01;1861(2):148141.

24. Yamamoto H, Shikanai T (2019) PGR5-Dependent Cyclic Electron Flow Protects Photosystem I under Fluctuating Light at Donor and Acceptor Sides. *Plant Physiol* 179(2):588–600.

25. Sunil B, Saini D, Bapatla RB, Aswani V, Raghavendra AS (2019) Photorespiration is complemented by cyclic electron flow and the alternative oxidase pathway to optimize photosynthesis and protect against abiotic stress. *Photosynth Res* 139(1–3):67–79.

26. Mosebach L, Heilmann C, Mutoh R, Gäbelein P, Steinbeck J, Happe T, et al (2017) Association of Ferredoxin:NADP+ oxidoreductase with the photosynthetic apparatus modulates electron transfer in Chlamydomonas reinhardtii. *Photosynth Res* 134(3):291–306.

27. Buchert F, Mosebach L, Gäbelein P, Hippler M (2019) PGR5 is required for efficient Q cycle in the cytochrome b_6f complex during cyclic electron flow. bioRxiv 854489.

28. Nawrocki WJ, Bailleul B, Cardol P, Rappaport F, Wollman FA, Joliot, P (2019) Maximal cyclic electron flow rate is independent of PGRL1 in *Chlamydomonas*. *Biochim. Biophys. Acta - Bioenerg.* 1860, 425–432.

29. Rantala S, Lempiäinen T, Gerotto C, Tiwari A, Aro E-M, Tikkanen M (2020) PGR5 and NDH-1 systems do not function as protective electron acceptors but mitigate the consequences of PSI inhibition. Biochimica et Biophysica Acta (BBA) – *Bioenergetics* 1861(3):148154.

30. Gerotto C, Alboresi A, Meneghesso A, Jokel M, Suorsa M, Aro E-M, et al (2016) Flavodiiron proteins act as safety valve for electrons in Physcomitrella patens. *Proc Natl Acad Sci* .

31. Steinbeck J, Ross IL, Rothnagel R, Gäbelein P, Schulze S, Giles N, Ali R, Drysdale R, Sierecki E, Gambin Y, Stahlberg H, Takahashi Y, Hippler M, & Hankamer B (2018) Structure of a PSI-LHCI-cyt b_6f supercomplex in *Chlamydomonas reinhardtii* promoting cyclic electron flow under anaerobic conditions. *PNAS* 115(41): 10517–10522.

32. Baniulis D, Zhang H, Zakharova T, Hasan SS and Cramer WA (2011) Purification and crystallization of the cyanobacterial cytochrome b6f complex. Photosynthesis Research Protocols. Methods in Molecular Biology (Methods and Protocols), 684, 65-77 Humana Press, Totowa, NJ

33. Sreerama N, Woody RW. Estimation of Protein Secondary Structure from Circular Dichroism Spectra: Comparison of CONTIN, SELCON, and CDSSTR Methods with an Expanded Reference Set. *Analytical Biochemistry* 287(2):252–60.

34. Yan J, Kurisu G, Cramer WA (2006) Intraprotein transfer of the quinone analogue inhibitor 2,5-dibromo-3-methyl-6-isopropyl-p-benzoquinone in the cytochrome b_6f complex. Proc Natl *Acad Sci* 103(1):69.

35. Freire E, Mayorga OL, Straume M (1990) Isothermal titration calorimetry. Anal Chem. [Google Scholar]

36. Tellinghuisen J (2007) Calibration in isothermal titration calorimetry: heat and cell volume from heat of dilution of nacl(aq). *Anal Biochem* 360(1):47-55.

37. Roberts AG, Bowman MK, Kramer DM (2004) The inhibitor DBMIB provides insight into the functiona architeture of the Qo site in the cytochrome b6f complex. *Biochemistry* 43, 24, 7707–7716.

VITA

EDUCATION

Purdue University, West Lafayette, IN
Master of Science in Biological Sciences (*Structural, Biophysical and Computational Biology), 2020*
Bachelor of Science in Biochemistry, 2018

RESEARCH AND LABORATORY EXPERIENCE

Research Assistant, Dr. William Cramer laboratory, Purdue University 2015-2020

- Designed and implemented a project to perform mutagenesis, structural analysis on the proposed rate-limiting step associated with the cytochrome b_6f integral membrane complex of the photosynthetic electron transport chain (publications below).
- Measure the binding affinity between the b6f complex and the cyclic pathway protein, PGRL1, using isothermal titration calorimetry (ITC)
- Communicate scientific data persuasively to peer-reviewed journals and conferences.
- Techniques: Cloning and PCR, electrophoresis, plasmid construction, *E. Coli* transformation, biolistic transformation, membrane protein purification (FPLC), enzyme kinetics, biophysical techniques (UV/Vis spectrophotometry, circular dichroism), X-ray crystallography.

Undergraduate/Graduate Teaching Assistant, Purdue University Spring 2015–Fall 2019

- Instruct molecular biology and introductory biology courses; mentor students outside the classroom.
- Set up and facilitate a wet-lab in which students complete a procedure that supplements the week's concept. Evaluate students' understanding through examination.

Sea Turtle Conservation 8-week Research Internship, Hainan Normal University, China Summer 2016

- Compiled biochemical and endocrinal data from green sea turtles and statistically analyzed the data to analyze the health status of turtles in the South China Sea.
- Rehabilitated emaciated and dehydrated sea turtles rescued from the illegal Hainan market.
- Traveled to the Ritz Carlton Hotel Sanya*, Yalong Bay* and Sheraton Hotel Wanning*, Shenzhou Peninsula* to develop a program to educate children on the importance of oceanic conservation.

SKILLS & LEADERSHIP EXPERIENCE

Python and SQL Programming Proficiency

Computation Courses *CS 595, CS 563, CS 177, Purdue University* Fall 2017–present

- Completed graduate-level python computation courses in computational biology and bioinformatics.
- Learned to utilize Biopython, perform object-oriented coding, database organization (SQL), and perform statistical analyses on bulk data sets.

Global Science Partners, Purdue University Spring 2016–Spring 2018

Mentor and Group Leader*, College of Science*

- Passionately promote cross-cultural communication and the understanding of the varying life experiences and cultures through a program in the College of Science.

Biology Ambassadors, Purdue University Spring 2017–Spring 2018

Volunteer Student Ambassador*, Department of Biology*

- Represented the department to prospective students at Purdue admission events.
- Presented my experiences to teach potential students how to be successful in their undergraduate career.

PUBLICATIONS

Ness, J., *et al*. (2019). Structure-based control of the rate limitation of photosynthetic electron transport. *FEBS* 593: 2103-2111. DOI: https://doi.org/10.1002/1873-3468.13484

Cramer WA, Ness J., Hasan S.S., *et al*. (2019). Structure-Based Change in the Rate-Limiting Step of Photosynthetic Electron Transport [abstract]. *Biophysical Journal* 116:154. DOI: https://doi.org/10.1016/j.bpj.2018.11.857

CONFERENCES

Presentation-talks

Biophysical Society Meeting, Baltimore, MD, 2019
Fifth Midwest Membrane Trafficking and Signaling Symposium, Purdue University, 2019
Midwest/Southeast 44th Photosynthesis Meeting, Indianapolis, 2019

Presentation-posters

Hitchhikers Guide to the Biomolecular Galaxy, Purdue University, 2019
Midwest/Southeast Photosynthesis Meeting, Indianapolis, IN, 2017 and 2018

NOTABLE AWARDS

- **Women in Science Travel Grant**, Purdue University, Spring 2019
- **Best Oral Presentation Conference Award,** Midwest/Southeast Annual Photosynthesis Meeting, October 2018
- **Biological Sciences Excellent Undergraduate Scholarship,** Purdue University, Spring 2017
- **Irwin And Ethel Tessman Scholarship Award**, Purdue University**,** Fall 2016